2021

Implementation of Model-Free Adaptive Power Flow Control for Dual-Active-Bridge-Based AC-DC Converters

Qinghang Shen
Minnesota State University, Mankato

IMPLEMENTATION OF MODEL-FREE ADAPTIVE POWER FLOW CONTROL FOR DUAL-ACTIVE-BRIDGE-BASED AC-DC CONVERTERS

By

Qinghang Shen

A Thesis Submitted in Partial Fulfillment of the

Requirements for the Degree of

Master of Science

In

Electrical Engineering

Minnesota State University, Mankato

Mankato, Minnesota

July, 2021

July 08, 2020

Implementation of model-free adaptive power flow control for dual-active-bridge-based AC-DC converters,

Qinghang Shen

This thesis has been examined and approved by the following members of the student's committee.

Prof. Vincent Winstead, advisor

Prof. Jianwu Zeng, committee member

Prof. Han-Way Huang, graduate coordinator

IMPLEMENTATION OF MODEL-FREE ADAPTIVE POWER FLOW CONTROL FOR DUAL-ACTIVE-BRIDGE-BASED AC-DC CONVERTERS

Qinghang Shen

Advisor: Dr. Vincent Winstead

MINNESOTA STATE UNIVERSITY, MANKATO

MANKATO, MINNESOTA

July, 2020

ABSTRACT

With the rising energy consumption and environment destruction problems worldwide, the development of renewable energy and energy recapture methods to improve the energy utilization rate has become more important as two of the most efficient processes to solve those problems. Bidirectional AC/DC converter and its modulation strategies are widely used as the essential part of implementing bidirectional power conversion between power grid and energy storage systems. To improve the efficiency and accuracy of the power conversion within AC/DC converters, a stable, robust power flow control system with quick response and disturbance rejection ability is desired.

This thesis proposes a model-free adaptive power flow control system based on a single-stage dual-active-bridge-based (DAB Based) AC/DC converter system with single H-bridge phase shift modulation (SHBM). The working states of DAB AC/DC converter under SHBM and implementation process of Compact-Form Dynamic Linearization Model-Free Adaptive Control (CFDL-MFAC) are presented to build the structure of the control system. Implementation details such as controller parameters, evaluation indexes etc. are discussed. Effectiveness and stability of this power flow control system are validated by simulation experimental results. Compared with the commonly used PID power flow control system, the proposed system has quicker response time for the continuous power changes, better control performance and stronger disturbance rejection capability.

ACKNOWLEDGMENTS

Studying in a foreign country and working on several new research topics in the past two years has been such a challenging adventure for me, especially under the impact of Covid-19. But I feel proud and grateful that I had the chance to be part of Dr. Winstead's research team and work on various research topics, including communication system, hardware development and converter control, at this point.

Firstly, I would like to thank my academic and research advisor, Dr. Vincent Winstead, who has given me the most guidance and support on my research and has always been patient with me. More important, he showed me how to be a good researcher. Secondly, financial support from the Xcel Energy through the Renewable Development Fund is gratefully acknowledged. I would not have had the chance to study in the US without their generous help. Thirdly, I want to say "thank you" to the professors in ECET department who have provided numerous amazing courses and helped me with my research work in any way they could. In addition, I would like to express my gratitude to my committee members, Dr. Han-Way Huang and Dr. Jianwu Zeng, for their advice on my work. Last but not least, I need to thank my parents and friends. They have always been supportive to all of my decisions and offered me constant mental guidance. In short, I am grateful for all the people that helped me to pull through this tough but inspiring experience.

TABLE OF CONTENTS

LIST OF TABLES

LIST OF ACRONYMS

Acronym	Full Name
RESs	Renewable Energy Sources
ESS	Energy Storage Systems
PFC	Power Factor Correction
PSM	Phase Shift Modulation
SPS	Single-Phase Shift Modulation
ESPS	Extended Single-Phase Shift Modulation
DPS	Dual-Phase Shift Modulation
TPS	Triple-Phase Shift Modulation
DAB	Dual-Active-Bridge
TPZM	Trapezoidal Modulation
DHBM	Dual H-Bridge Modulation
SHBM	Single H-Bridge Modulation
MFAC	Model-Free Adaptive Control
PDD	Pseudo Partial Derivative
CFDL	Compact-Form Dynamic Linearization
PG	Pseudo Gradient
PFDL	Partial-From Dynamic Linearization
PJG	Pseudo Jacobian Matrix
FFDL	Full-Form Dynamic Linearization
ZCS	Zero-Current Switching

ZVS	Zero-Voltage Switching
SISO	Single Input Single Out
BIBO	Bounded Input Bounded Output
ITAE	Time Multiply by Absolute Error Index
PID	Proportion-Integral-Derivation

LIST OF VARIABLES

Variable	Meaning
S	Two-Quadrant Switch
V_{AC}	AC Voltage Source from the Power Grid
V_{ac}	RMS Value of AC Source
$v_{ac}(t)$	Voltage Value of AC Source
V_{DC}	DC Voltage Source from the ESS
v_{dc}	Voltage Value of DC Source
L_1	Inductance of the LC Filter Circuit on AC Side
L_2	Leakage Inductance of the Transformer
C	Capacity of the LC Filter Circuit on AC Side
n_t	Turn Ratio of the Transformer
t	Time
T_s	Switching Period of the DAB AC/DC Converter
f_s	Switching Frequency of the DAB AC/DC Converter
v_p	Primary Side Voltage of the Converter
d	Duty Cycle on the Primary Side
d_{dc}	Duty Cycle on the Secondary Side
δ	Phase Shift Ratio
v_s	Secondary Side Voltage of the Converter
v_L	Leakage Inductor Voltage
i_L	Leakage Inductor Current

$e(k)$	Error Signal between Reference and Output Signal
$P_{\text{active\_ref}}$	Active Power Flow Reference Signal
P_{active}	Current Output Active Power Flow Signal
K_p	Proportion Parameter
K_i	Integral Parameter
K_d	Derivation Parameter
$y(k)$	k_{th} Output
$u(k)$	k_{th} Input
$\phi_c(k)$	k_{th} PPD
λ	Weighting Factor of Control Law
μ	Weighting Factor of PPD Estimation Equation
ρ	Step Factor of Control Law
η	Step Factor of PPD Estimation Equation
$z(k)$	Filtered Error Signal
$L(q)$	Transfer Function of Error Filter
I	ITAE Value
$d(k)$	Load Disturbance
$w(k)$	Measurement Disturbance

Note: Variables dependent on t are continuous and variables dependent on k are discrete.

Chapter 1: Background and Introduction

1.1 Background

With the rapid rise of population and the development of technologies in various industries, the demand of energy consumption worldwide has tremendously increased in the last two decades. Meanwhile, with the sharp reduction of the supply of fossil fuels like oil, coal and other non-renewable reserves, and the serious environmental pollution and destruction caused by exploiting the fossil fuel sources, insufficient resources have become a severe problem for mankind around the world. Thus, solving the energy problem has priority and has gradually become a hot research topic in the international community.

[1] states that the development of renewable energy such as solar energy, wind energy etc. and energy recapture to improve the energy utilization rate are regarded as two of methods having the most potential to solve the energy problem at present. Research and application over renewable energy sources (RESs) has been widely performed in different fields and already made some progress in last 20 years. As for energy recapture, Energy Storage Systems (ESS) using DC battery packs with feedback has become a hot research topic in the energy industry. Bidirectional AC/DC converters are one of the most important parts of the “ESS with feedback energy”. They could realize the bidirectional energy transmission in the DC side of the ESS and the AC side of the power grid, which means power could flow from the grid to ESS equipment when it is charging and flow back to the grid to realize energy recapture, and greatly improve the efficiency of power usage, while storing unneeded energy waste. The general working mode of bidirectional AC/DC converter between “ESS with feedback energy” and power grid is shown in Fig. 1.1.

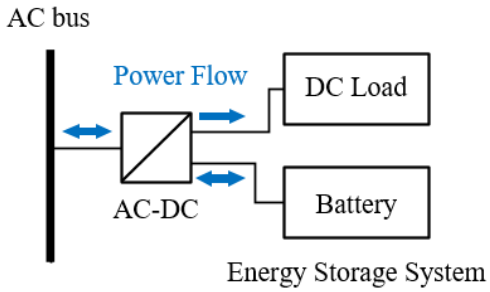

Fig. 1.1 Bidirectional AC/DC Converter System

The figure shows that a bidirectional AC/DC converter enables bidirectional power transmission between the power grid and ESS such as a battery pack, however, the direction and magnitude of power flow will be influenced by various factors. Inappropriate power flow may cause low energy utilization rate and non-functionality of appliances. In this case, proper modulation and control strategies should be performed on the power flow to achieve efficient utilization and energy recapture.

1.2 Introduction to AC/DC Converter and its Modulation Strategies

1.2.1 Bidirectional AC/DC Converter

Bidirectional AC/DC converter is a kind of power electronic system that enables voltage conversion and bidirectional energy transmission under different circumstances. It is commonly used in combination with battery systems, energy storage devices, hybrid wind-solar systems, electric vehicles and hybrid vehicles along with other applications, which could implement energy recapture between power grid and energy storage units. According to the state of input and output, a bidirectional AC/DC converter is supposed to work in both rectifier and inverter mode:

(1) When energy needs to be transferred from the AC grid side to the DC ESS side, the converter needs to work in the rectifier mode. At this point, the converter converts the periodic, fluctuating AC power into constant DC power. For DC side ESS and other DC devices, stable DC power flow is indispensable for their functionality.

(2) When energy needs to be fed back from the DC ESS side to the AC grid side, the converter needs to work in the inverter mode. At this point, the converter converts DC power stored in ESS into AC power fed back to the AC grid. This process realizes energy recapture and improves efficiency.

The most widely used bidirectional AC/DC converter topology right now, which is mentioned in [2], is composed of an active Power Factor Correction (PFC) circuit in the front stage and a dual-active-bridge circuit in the back stage, which is shown in Fig. 1.2. The PFC circuit is used for power factor correction, and the dual active bridge circuit enables adjustment on the output voltage and current. The topology is easy to realize and control.

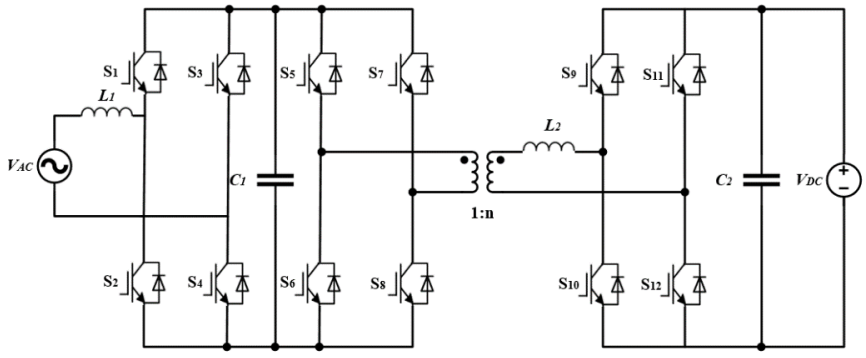

Fig. 1.2 Traditional Bipolar AC/DC Converter Topology

However, due to the series connection of two stages, the efficiency of this topology is relatively low. In addition, as statements in [3], the DC bus voltage between those two

bridges requires large capacitance C_1, which will increase the size of the converter and the production cost. To improve efficiency and power density, various single-stage topologies has been developed. The Dual-Active-Bridge Converter (DABC) was proposed in the early 1990s and has been widely used since because of its simple and symmetrical structure, transformer isolation, large soft-switching interval, strong bidirectional power transmission, low device stress and small filter requirements. These make them suitable for applications requiring high power density. It is composed of two half-bridge topologies connected by a transformer and a series inductor. In [4], researchers proposed a single-stage dual-active-bridge-based (DAB-based) bidirectional AC/DC converter topology, which is shown in Fig. 1.3 and employs four-quadrant switch to replace the traditional DC/DC dual-active-bridge converter and the full-bridge topology as the input of AC side.

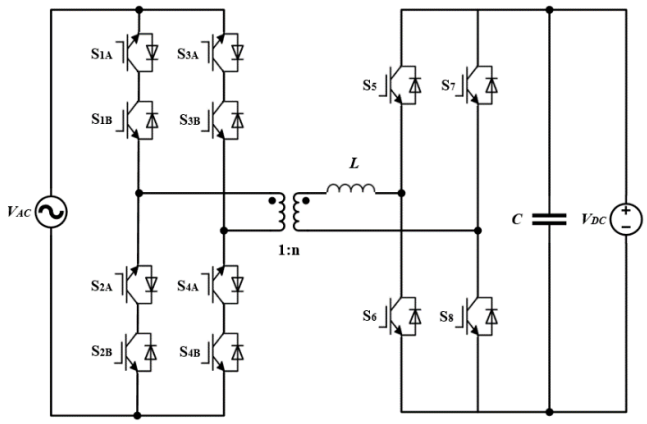

Fig. 1.3 Single-stage Dual-active-bridge-based Bidirectional AC/DC Converter Topology

Compared with the two-stage scheme using the active power factor correction, the single-stage scheme has the advantages of fewer components, high power density and high transmission efficiency. So, in this design, we employ this topology as our objective to

perform modulation and control experiments. Details about the figures and parameters will be introduced in chapter 2.

1.2.2 Power Flow Modulation Strategies

Since bidirectional AC/DC converter is commonly used as the bridge that connects power grid and ESS equipment, it should provide steady, accurate and constant power to the grid and EES when it works in both rectifier and inverter modes. In this case, power flow control has become an active research area when generalizing the application field of bidirectional AC/DC converters. Generally, there are two factors that need to be under consideration in power flow control: direction and magnitude. The key capability allows one to adjust the magnitude and direction of power flow dynamically to stratify the consumption needs from both grid and ESS side, so as to improve the efficiency.

For the single-stage DAB AC/DC converter topology used in the target design, where one implements the power flow control for bidirectional energy transmission, phase shift modulation (PSM) is the most common strategy. The essential methodology of PSM is modulating the phase relationship of the voltage on both sides of the bridge within the converter to adjust the direction and magnitude of the leakage inductor current to control the active power flow. In [5], PSM strategy is mainly categorized into four distinct operating modes: single-phase shift (SPS) modulation, extended single phase shift (ESPS) modulation, Dual-phase-shift (DPS) modulation and triple phase shift (TPS) modulation.

The SPS modulation mode is the most commonly used modulation strategy, in which the upper and lower bridges are complementary to each other, and a nonzero phase shift angle exists between the primary and second H-bridge switching waveforms. Meanwhile, both the

primary and secondary H-Bridges are modulated with 50% duty cycle and the active power could be controlled by adjusting the phase shift between these two H-bridges according to the statements in [6]. This modulation method is simple to control and easy to implement, however, limiting the control to one degree of freedom resulting in poor efficiency in no-load situation, massive reactive current flow, and restricted soft switching range when the variation of input–output voltages is wide as statements in [7]. This problem is usually solved by adding more degrees of freedom into PSM. This concept has led to more improved PSM strategies.

The ESPS modulation mode adds another degree of freedom by including the pulse width variation of one side of the H-bridge based on SPS modulation, which reduces the circulating energy and the conduction losses for medium power. The DPS modulation mode is an improvement of ESPS, which includes the pulse width variation of both sides of the H-bridge. Since the variation values on both sides of the H-bridge are the same, it has better dynamic performance when changing the direction of power flow.

The TPS modulation mode is an improvement based on DPS, which has different pulse width variation on the two side H-bridges and increases the degrees of freedom to three. It usually has the best control performance. However, it is also hard to implement. Trapezoidal modulation (TPZM) or dual H-bridge modulation (DHBM) has three degrees of freedom, variable duty cycles for both the bridges and the phase shift angle between the AC and DC side switch waveforms. Duty cycle modulation of only one/single H-Bridge (SHBM) was introduced in [9] and further studied in [10], [11] to obtain wider soft-switching range and improve efficiency.

All the improved modulation strategies aim to optimize the control performance of PSM, but one problem still remains. Since the active power is a nonlinear function of the control variable (such as phase shift angle or duty cycle), in most modulation strategies, extra control actuation is needed to control the active power flow in order to further improve power efficiency. Since the relationship is nonlinear and an accurate mathematical model of the converter system is hard to obtain in real-world applications, most of the model-based control strategies cannot be applied effectively under this circumstance. So based on existing modulation strategies, this design is going to apply a proper control system and strategy to control the active power flow efficiently and quickly.

1.2.3 Model-Free Adaptive Control

Model-Free Adaptive Control (MFAC) theory was firstly proposed by Zhongshen Hou in 1994 in [12]. This method of controller design only uses the I/O data of the controlled system, excluding any model information of the system, and can achieve the parameter adaptive and structural adaptive control of system, which yields a model-free and data-driven control method.

In [12], for MFAC, instead of generating a explicit nonlinear model of a system, a virtual equivalent dynamical linearization data model is identified at each dynamic operating point of the closed-loop system using the dynamic linearization technique with a novel concept called Pseudo Partial Derivative (PPD). With using the equivalent virtual data model, adaptive control of the nonlinear system could be implemented by a proposed controller.

Compared with traditional adaptive control schemes, the MFAC approach has several advantages, which make it more suitable for many practical control applications.

1) MFAC is a pure data-driven control method. This control method only depends on the real-time measurement I/O data of the controlled system, without using any model derived information of the system. This indicates that a general controller that could fit many practical industrial processes could be designed independently.

2) MFAC does not require any external testing signals or any training process. This process is usually necessary for neural network-based nonlinear adaptive control. Therefore, the computational cost of implementing MFAC is lower than other controllers.

3) MFAC could be easily implemented with little computational burden and the control method has strong robustness. Stability and robustness of MFAC has been discussed in prior work [13], which proves it is stable and robust in most situations.

At present, MFAC has been successfully applied in the fields of oil refining, chemical industry, electric power, light industry and urban expressway traffic inflow ramp control as statements in [14] and has demonstrated in industry good performance on solving control problems when the model is hard to obtain, or the relationship is non-linear. Further studies about application of MFAC could be found in [15], which makes it a good match with the power flow control system utilized in this design.

1.3 Review of Prior and Related Work

The power flow control of DAB AC/DC converter could be configured in two ways: 1) Phase Shift Modulation (PSM) by using the nonlinear relationship between the active power flow and control variables within the converter; 2) Converter Control Strategies by optimizing the control variables to obtain the desired active power flow.

A number of extensions to the basic PSM control methodology have been proposed in the literature to improve the performance of converters. In [16], the parameters of TPZM, two duty cycles and the phase shift are optimized to achieve minimum inductor and transformer rms current for a DAB converter. In [4] and [17], Triangular modulation (TRM) is proposed as a special case of TPZM where at one transition in every half cycle both the input and output bridges are switched together resulting in a triangular shape current waveform. In [18] and [19], PSM, TRM, and TPZM are combined together to a hybrid modulation in order to achieve optimal efficiency over a wide operating range. In [20], a modulation scheme combining phase shift and frequency modulation of DAB AC/DC converter that can achieve unified power factor and full range soft switching was proposed. However, the optimization steps must be repeated at all power levels, which yields complex algorithmic computations. In [21] and [23], a special case of SHBM has been identified as inner mode and shown to achieve zero-current switching (ZCS) in one of the bridges as well as a simple linear power relationship. This enables various control strategies to continue working on the modulation. Although modulation strategies are extensively explored in the literature, the control methods to apply for the modulation leading to improved performance are not widely used.

For the control strategies method, the research on this field mainly includes grid-less electromotive force proposed by B. H. Kwon in [22], the control strategy of current sensor, the control strategy based on Lyapunov stability, the optimal control strategy of voltage response time, and the admittance feedforward compensation control strategy. Among them, the current control algorithm receives considerable interest in current research and in application related to power flow control, which allows power flow control through current

control. At present, the most commonly used current control algorithm in bidirectional AC/DC converter is the classical PID algorithm. However, other algorithms yielding improved performance are also employed, including hysteresis control, predictive control, fuzzy control, single cycle control and sliding mode control and among other methods. For fuzzy control, one does not need to establish an accurate mathematical model of the converter, which removes the need for an extensive modeling process when it is difficult to obtain a mathematical model. Therefore, in the case of complex circuit topology, fuzzy control is getting more and more attention. For sliding mode control, the advantage is that it can maintain good stability and robustness under uncertain system parameters. From those algorithms, one can tell the research topic related to current control of bidirectional AC/DC converter involves model-free control algorithms with good stability and robustness.

1.4 Research Objectives

Inspired by thorough research on multiple topologies and advanced figures, like soft switching, power factor correction etc., of DAB AC/DC converter, various phase shift modulation strategies and model-free adaptive control algorithm have been validated in many applications. The idea of building a stable, robust power flow control system based on the phase shift modulation strategy for DAB AC/DC converter and model-free adaptive controller to enable the converter to make quick, accurate responses on the changing power consumption needs of the grid and EES transients and improve the power efficiency of bidirectional power conversion can be achieved through the following three objectives.

1) Quick and Accurate Response Ability. If power flow from the grid or the EES equipment are time-varying, wrong or is insufficient, it could lead to power loss or even

damage of EES equipment. The converter is supposed to adjust the conversion operating point based on the requirements from input and output sides quickly and accurately to maximum the power efficiency and ensure the functionality of appliances.

2) High Stability and Robustness. No matter what the grid or the EES appliance requires, one expects a stable power flow under any circumstance. However, disturbances are unavoidable in the real-world, so the controlled converter system is supposed to be stable, reliable and robust under most applications.

3) Disturbance Rejection Capability. Besides impacts to stability and robustness, disturbances from various sources could lead to inaccuracy of the magnitude of power flow which will directly influence the efficiency of the converter system. So certain disturbance rejection capability is required for the designed control system.

1.5 Outline of Thesis

Following the above introductions, an outline of this thesis is stated as follows.

Chapter 2 introduces the Dual-Active-Bridge-Based AC/DC converter which will be the controlled subsystem in the designed system. The topology, characteristics, working process and modulation strategy for the inner power flow mechanisms are discussed. The control methodology for power flow within DAB AC/DC converter is proposed at the end of this chapter.

Chapter 3 proposes two different controllers with their control schemes, respectively, and describes the Model-Free Adaptive Control (MFAC). The methodology, category and main figures are presented. Some modification made on MFAC and the major concerned

problems when applying the MFAC are also discussed in detail for the purpose of improving the performance of MFAC.

Chapter 4 shows the results of a series of simulations and results to verify the functionality, stability and robustness of controlled systems. Comparison and analysis are performed on the simulation results of the experiments designed to compare two control methods and provide some details and conditions about simulations towards achieving better controller performance. Finally, this thesis ends with some conclusions, a summary of the work that has been done and some recommendations for future work in Chapter 5.

Chapter 2: Dual-Active-Bridge-Based AC/DC Converters

2.1 Topology and Features

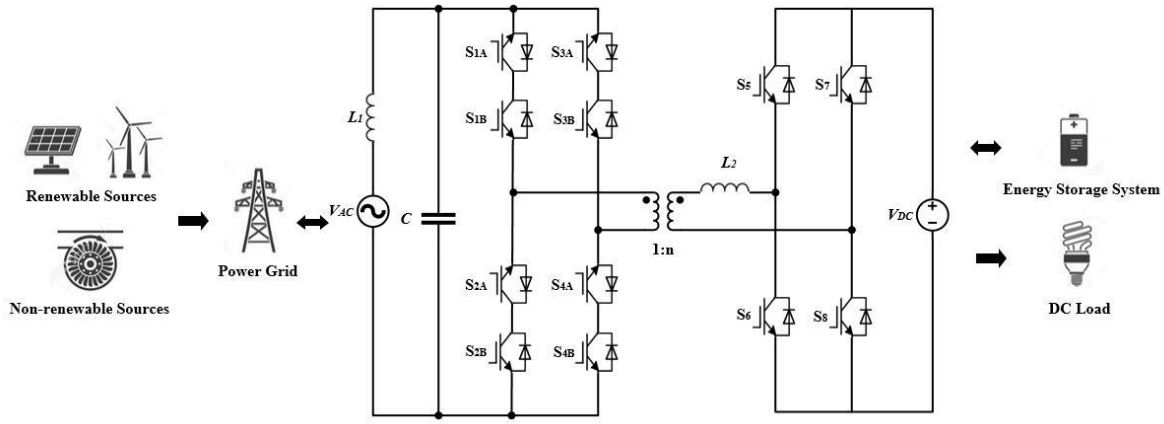

Fig. 2.1 Topology of the DAB AC/DC converter

Fig. 2.1 shows the topology of the single-stage Dual-Active-Bridge-Based AC/DC converter. The AC side of the converter is connected to the AC bus of the power grid, which transmits power generated by renewable and non-renewable sources. The DC side is connected directly to the DC load or energy storage system such as a battery pack. Main components of the converter are: four four-quadrant switches S_1, S_2, S_3 and S_4, four two-quadrant switches S_5, S_6, S_7 and S_8, and one transformer. The capacitors C and inductor L_1 on the AC side compose the LC circuit to filter the voltage waveform. The transformer whose turns ratio is defined as $n_t = n/1$ is modeled as an ideal transformer in series with a leakage inductor L_2 on the secondary side.

In [21], this single-phase DAB AC/DC converter topology was thoroughly studied and proved to be functional. In [23], the topology is further explored with a modulation technique based on inner mode of SHBM, which will also be the fundamental modulation strategy for

the power flow control system built in this design. The single-stage DAB AC/DC converter under the inner mode SHBM modulation purports to achieve the following advantages:

1) Galvanic isolation;
2) Single-stage power conversion and bi-directional power flow;
3) Open-loop Power Factor Correction (PFC);
4) Zero-Current Switching (ZCS) for the primary side H-bridge in all load conditions;
5) Zero-Voltage Switching (ZVS) for the secondary side H-bridge;
6) The reactive power is proportional to the phase shift.

Those features make the application of power flow control system possible. Although under the modulation of the inner mode SHBM, the active power could be linear in the control variable, although this is just a special case. In real-world, the model of this relationship is hard to obtain, and with other modulation strategies, active power is nonlinear in the control variable. So, a model-free control algorithm with the ability to accommodate nonlinear systems is desired for power flow control under this circumstance.

2.2 Converter Operation with SHBM

For single-stage DAB AC/DC converter, there are usually two working states, either working as a rectifier or inverter. When the power flows from the power grid to the EES, the converter works as a rectifier, which converts the AC power to DC power, and we assume this is the forward direction, which indicates the sign of the power value is positive. When the power flows from the EES to the power grid, the converter works as an inverter, which converts the DC power into the AC power. This is the backward direction, so the sign of the power value is negative.

For Single H-Bridge Modulation (SHBM), there are two degrees of freedom. They are the duty cycle of the switching waveform of the DC-side H-Bridge and the phase shift between the switching waveform between on the AC-side and DC-side, respectively. For those two parameters, when duty cycle is fixed, active power flow will be controlled by the phase shift. In the following section, the converter's two working states are analyzed which are forward and backward power flow, respectively, under the modulation of SHBM. In the following analysis, all the switches are considered to be ideal. As for the transformer, the magnetizing inductance, winding resistances and cores losses are all neglected.

2.2.1 Forward Power Flow Working State

In the forward power flow working state, the converter works as a rectifier where power flows from the grid to EES. The AC-side source is defined in 2.1as

$$v_{ac}(t) = V_{ac}\sin(2\pi f_{ac}t), \tag{2.1}$$

where V_{ac} is the amplitude and f_{ac} is the frequency of AC source, respectively. The switches on the AC-side H-bridge is switched under the control of a quasi-square wave on the primary side of the transformer, which has frequency of f_s, period of $T_s = 1/f_s$ and duty cycle of 50%. So, the voltage of the transformer's primary side, v_p will be as shown in 2.2.

$$v_p(t) = \begin{cases} v_{ac}; 0 \le t < \dfrac{T_s}{2} \\ -v_{ac}; \dfrac{T_s}{2} \le t < T \end{cases} \tag{2.2}$$

The switches of DC-side H-Bridge on the secondary side of the transformer is controlled by a voltage pulse. The duration of the pulse signal is set by the duty ratio *d*, defined

in equation 2.3, and is phase shifted by the time quantity Δt . [23] proposes that given v_{ac} and V_{dc}, n is supposed to be chosen by keeping d less than unity.

$$d(t) = \frac{n|v_{ac}(t)|}{v_{dc}}, \tag{2.3}$$

The phase shift Δt is limited so that pulse of V_{dc} applied to the secondary side voltage of transformer, v_s, could remain within its respective $T_s / 2$ period, which results in

$$|\Delta t| \le \frac{T_s}{4}(1-d). \tag{2.4}$$

The phase shift ratio δ is defined in equation 2.5. The maximum duty ratio d is defined in equation 2.6. The phase shift ratio δ has a range of $-\left(1-\hat{d}\right)$ to $\left(1-\hat{d}\right)$ where

$$\delta = \frac{\Delta t}{T_s / 4}, \tag{2.5}$$

$$\hat{d} = \frac{nV_{ac}}{v_{dc}}, \tag{2.6}$$

$$|\delta| \le 1-\hat{d}. \tag{2.7}$$

Assuming the turns ratio of transformer is 1:1, which means $n=1$, it follows that from equation 2.6 and 2.7, the input voltage peak needs to be less than the output voltage magnitude in order to have reasonable phase shift.

If we divide one period T_s into 5 intervals by six time points $t_i : i \in \{1, 2, \ldots, 6\}$, which is defined in equation 2.8. Then the voltage v_s applied by the dc-side H-bridge is defined for one cycle of in equation 2.9, where λ is defined as the $\operatorname{sgn}\left(v_{ac}(t)\right)$.

$$\begin{cases} t_1 = \dfrac{T_s}{4} - \left(\dfrac{dT_s}{4} - \dfrac{\delta T_s}{4} \right) = \dfrac{T_s}{4}(1+\delta-d); \\ t_2 = \dfrac{T_s}{4} + \left(\dfrac{dT_s}{4} + \dfrac{\delta T_s}{4} \right) = \dfrac{T_s}{4}(1+\delta+d); \\ t_3 = \dfrac{T_s}{2}; \\ t_4 = \dfrac{3T_s}{2} - \left(\dfrac{dT_s}{4} - \dfrac{\delta T_s}{4} \right) = \dfrac{3T_s}{2} + \dfrac{T_s}{4}(\delta-d); \\ t_5 = \dfrac{3T_s}{2} + \left(\dfrac{dT_s}{4} + \dfrac{\delta T_s}{4} \right) = \dfrac{3T_s}{2} + \dfrac{T_s}{4}(\delta+d); \\ t_6 = T_s. \end{cases} \tag{2.8}$$

$$v_s(t) = \begin{cases} 0; 0 \le t < t_1 \\ \lambda v_{dc}; t_1 \le t < t_2 \\ 0; t_2 \le t < t_4 \\ -\lambda v_{dc}; t_4 \le t < t_5 \\ 0; t_5 \le t < t_6 \end{cases} \tag{2.9}$$

Therefore, the waveform of v_p and v_s in one period T_s is shown in Fig. 2.2.

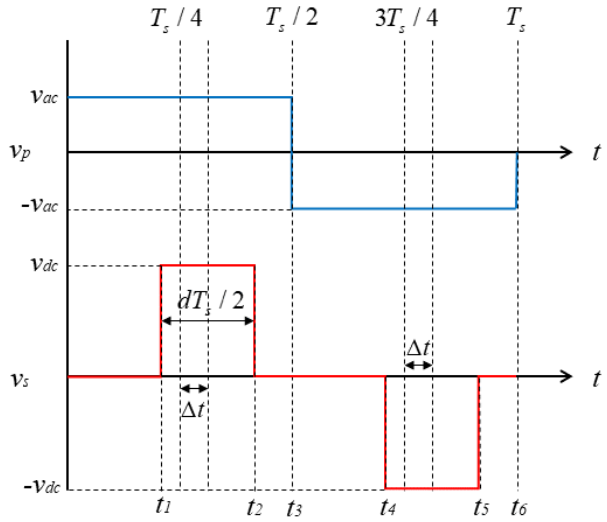

Fig. 2.2 Waveform of v_p and v_s in One Period T_s

Using the voltage at v_p, v_s and the turns ratio of the transformer, the voltage across the inductor, $v_L(t)$ in equation 2.10, is calculated for one complete cycle of T_s period in equation 2.11, and the waveform is shown in Fig. 2.3.

$$v_L(t) = nv_p(t) - v_s(t) = L_2 \frac{di_L}{dt}, \tag{2.10}$$

$$v_L(t) = \begin{cases} nv_{ac}; 0 \le t < t_1 \\ nv_{ac} - \lambda v_{dc}; t_1 \le t < t_2 \\ nv_{ac}; t_2 \le t < t_3 \\ -nv_{ac}; t_3 \le t < t_4 \\ -nv_{ac} + \lambda v_{dc}; t_4 \le t < t_5 \\ -nv_{ac}; t_5 \le t < t_6 \end{cases} \tag{2.11}$$

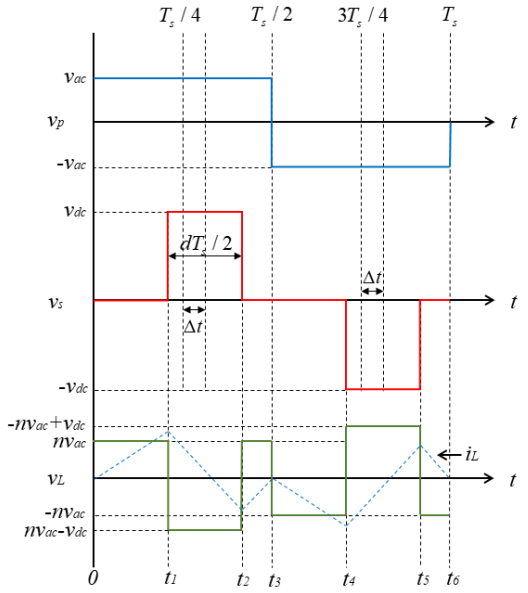

Fig. 2.3 Waveform v_L and i_L in One Period T_s

And the four different working stages for forward power flow are shown in Fig. 2.4.

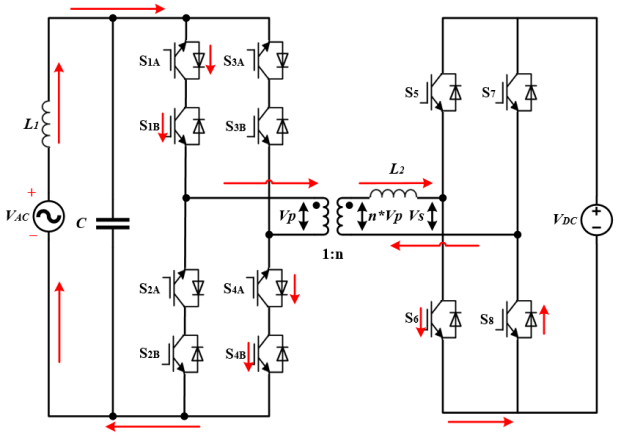

(a) $0 \le t < t_1$ and $t_2 \le t < t_3$, S_7 is in open state, S_8 in ZVS, $v_s = 0$;

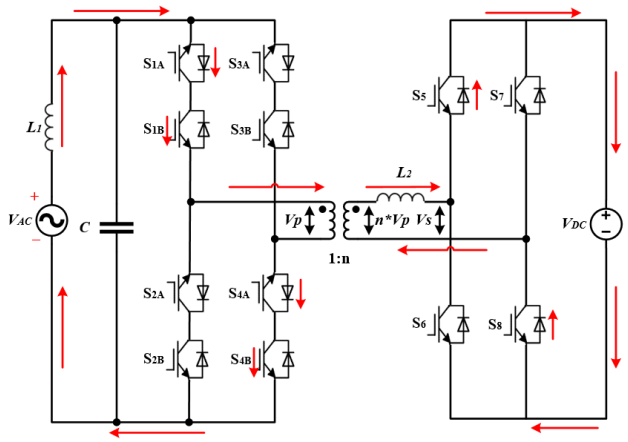

(b) $t_1 \leq t < t_2$, S_6 is in open state, S_5 in ZVS, DC-side is charging;

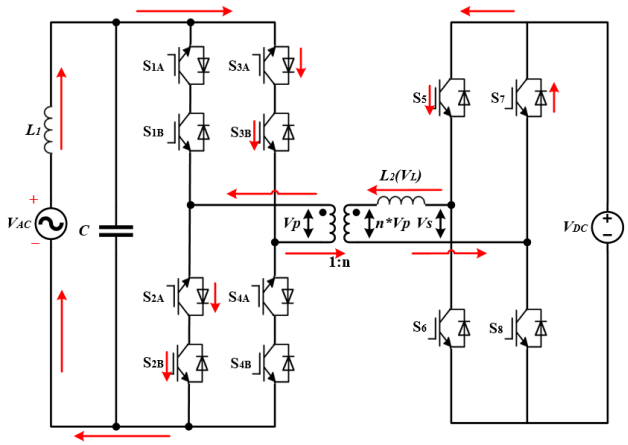

(c) $t_3 \leq t < t_4$ and $t_5 \leq t < t_6$, S_8 is in open state, S_7 in ZVS, $v_s=0$;

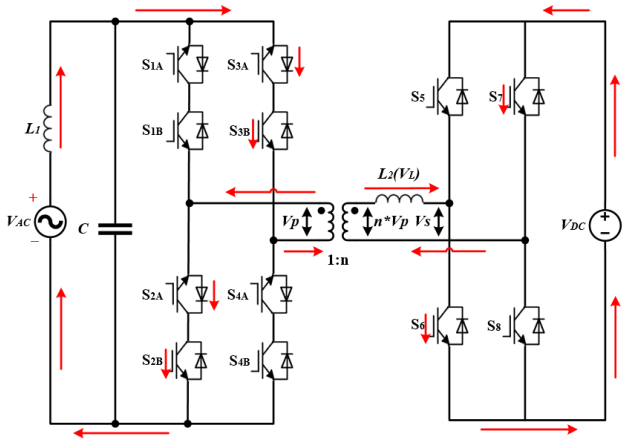

(d) $t_4 \leq t < t_5$, S_5 and S_8 is in open state, S_6 and S_7 conduct.

Fig. 2.4 Four Working Stages of Converter Under Forward Power Flow

From equations 2.10 and 2.11, the voltage across the leakage inductor v_L is time-varying and influenced by duty cycle d and phase shift ratio δ. The current i_L through the leakage inductor is associated with v_L. Since i_L determines the active power flow, then with fixed d, we could control the active power flow by modulating phase shift ratio δ. The relationship between them is nonlinear.

2.2.2 Backward Power Flow Working State

In the backward power flow working state, the converter works as an inverter and power flows from EES to the grid. Adjusting phase shift ratio δ from to $-\delta$ is the only controlled quantity in this system. Then if we divide one period T_s into 5 intervals $t_i : i \in \{1, 2, \ldots, 6\}$ where $T_s = \sum_{1}^{i} t_i$, which is defined in equation 2.12. Then the voltage v_s applied by the dc-side H-bridge is defined for one complete cycle of in equation 2.13, and the leakage inductor voltage v_L is defined for one period in equation 2.14.

$$\begin{cases} t_1 = \dfrac{T_s}{4} - \left(\dfrac{dT_s}{4} + \dfrac{\delta T_s}{4} \right) = \dfrac{T_s}{4}(1 - d - \delta); \\ t_2 = \dfrac{T_s}{4} + \left(\dfrac{dT_s}{4} - \dfrac{\delta T_s}{4} \right) = \dfrac{T_s}{4}(1 + d + \delta); \\ t_3 = \dfrac{T_s}{2}; \\ t_4 = \dfrac{3T_s}{2} - \left(\dfrac{dT_s}{4} + \dfrac{\delta T_s}{4} \right) = \dfrac{3T_s}{2} - \dfrac{T_s}{4}(d + \delta); \\ t_5 = \dfrac{3T_s}{2} + \left(\dfrac{dT_s}{4} - \dfrac{\delta T_s}{4} \right) = \dfrac{3T_s}{2} + \dfrac{T_s}{4}(d - \delta); \\ t_6 = T_s. \end{cases} \tag{2.12}$$

$$v_s(t)=\begin{cases}0;\ 0\le t<t_1\\ \lambda v_{dc};\ t_1\le t<t_2\\ 0;\ t_2\le t<t_4\\ -\lambda v_{dc};\ t_4\le t<t_5\\ 0;\ t_5\le t<t_6\end{cases} \tag{2.13}$$

$$v_L(t)=\begin{cases}nv_{ac};\ 0\le t<t_1\\ nv_{ac}-\lambda v_{dc};\ t_1\le t<t_2\\ nv_{ac};\ t_2\le t<t_3\\ -nv_{ac};\ t_3\le t<t_4\\ -nv_{ac}+\lambda v_{dc};\ t_4\le t<t_5\\ -nv_{ac};\ t_5\le t<t_6\end{cases} \tag{2.14}$$

And the waveforms of v_p, v_s, v_L and i_L in one period is shown in Fig. 2.5. The same nonlinear relationship between the phase shift ratio δ and leakage inductor current could also be applied on the backward power flow working stage, which enables the modulation on both active power flow direction and magnitude.

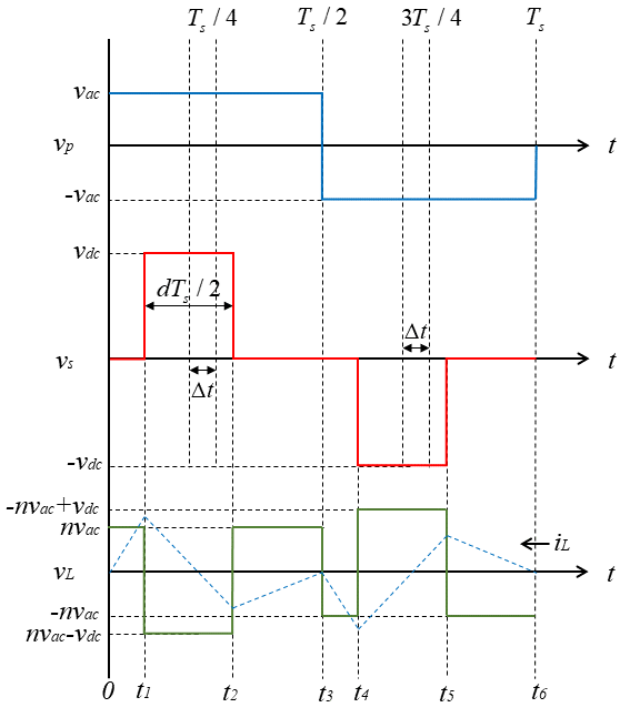

Fig. 2.5 Waveforms of v_p, v_s, v_L and i_L in One Period Ts

2.3 Control Goals

From the paragraph above, by applying single H-Bridge Modulation (SHBM) on the converter power flow, there is a linear relationship between the phase shift and active power flow when the duty cycles of both of the H-bridges are fixed. However, this is a special case, for most of the modulation strategies. This relationship is nonlinear under both forward and backward power flow situations. To generalize the power flow control system that is going to be designed, based on this nonlinear relationship, the magnitude and direction of the active power flow within the DAB AC/DC converter could be controlled, by modulating the magnitude and phase of the current. This is directly related to the phase shift. Thus, in this power flow control system, the input to the controller is the error between current active power and power demand. The output of the controller should be the phase shift. In order to choose the proper control structure, the features of the single-phase DAB AC/DC converter system have been summarized as follow:

1) The system is time-varying;
2) The system is single input single output (SISO);
3) The relationship between input and the output is generally nonlinear;
4) The mathematical model of this system is typically difficult to obtain in real-world;
5) The switching frequency within this system is relatively high.

The control method chosen should be based on the control goals and the features of this system. Since the mathematical model is hard to obtain, most of the model-based control methods will not be suitable in this case. Meanwhile, since the relationship is nonlinear, it is also complicated to build online model for this system. With those limitations, the first

feasible control method is the most commonly used method, PID control, which has already proved to be effective in many industrial situations to solve problems when the relationship is nonlinear and no mathematical model is required. Inspired by the research on adaptive control, the method of model-free adaptive control is able to work model-free and build a dynamic online model of this system that allows parameters to adapt which is a good solution for nonlinear models.

Chapter 3: Power Flow Control Methodology

3.1 DAB Converter Closed-loop Control Structure

In chapter 2, the control goals for the power flow control system were clarified, which is to control the active power flow within the signal-phase DAB AC/DC converter by modulating the phase shift, δ. In the control loop, the input will be the sampling error signal, e, which refers to the difference between reference active power, $P_{\text{active\_ref}}$, and current output active power, P_{active}, of the converter and is defined as equation 3.1 as follow.

$$e = P_{\text{active\_ref}} - P_{\text{active}}. \tag{3.1}$$

Then this signal will be delivered into the controller to produce the control signal of phase shift. Finally, the signal is applied to modulate the output active power by using the modulation strategy for DAB converter. The structure of the DAB closed control loop is shown in Fig. 3.1.

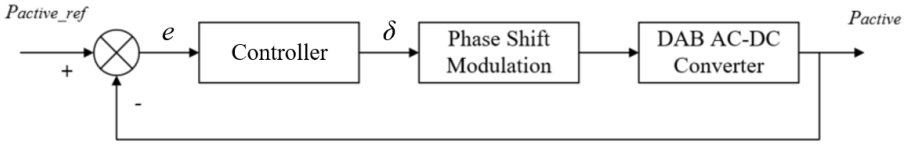

Fig.3.1 DAB Converter Closed-Loop Control Structure

3.2 PID Control

PID control is the most commonly used control method presently to solve different kinds of system control problems based on some of its features:

1) The Modulation of PID control is minimally dependent on the specific mechanism or mathematical model of the controlled system;

2) The structure of PID controller is simple, which makes PID control is easy to implement and can satisfy the control requirements for most of the practical problems;

3) PID control has good response to unmeasured disturbances leading to strong robustness, feasibility and adaptation.

Since the mathematical model of the DAB AC-DC converter is often difficult to obtain, PID control is an appropriate control method for this design. The basic structure of implementing PID control into the control loop is shown in Fig. 3.2.

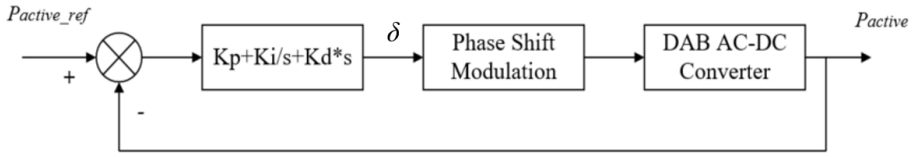

Fig. 3.2 Closed-Loop Control Structure with PID controller

For PID controller, *Kp, Ki*, and *Kd* stand for the coefficients of proportion, integration and differentiation, respectively. These coefficients decide the performance and efficiency of PID control which are usually determined through tuning guidelines, industry experience, trial and error or repeated calculation.

Above all, the essential part of implementing PID control is finding the proper PID regulator parameters based on the target control system. However, this process sometimes can be costly in time and resources. What's more, PID control also has some limitations when applied to some circumstances, such as applications with strong nonlinearity and difficulty in handling multiple variables with strong interaction. So, adequate performance of a PID controller for this design is not guaranteed.

3.3 Model-Free Adaptive Control (MFAC)

3.3.1 Control Structure with Model-Free Adaptive Control

Model-Free Adaptive Control (MFAC) with its model-free and data-driven control method fits our control requirement and system features very well. It only uses the I/O data of the controlled system without additional model information of the system, which enables this method to be parameter adaptive and structurally adaptive.

In [12], for the methodology of MFAC, at each dynamic operation point of the closed-loop system, a virtually equivalent dynamic linearization data model is generated by using a new dynamic linearization technique with novel concept called Pseudo Partial Derivative (PPD). The commonly used dynamic linearization techniques are Compact-Form Dynamic Linearization (CFDL) data model, Partial-Form Dynamic Linearization (PFDL) data model, and Full-Form Dynamic Linearization (FFDL) data model. These models are separately used in various circumstances based on the practical control problems. The main difference among them are the dynamic linearization techniques to construct the virtual equivalent dynamical linearization data model. For CFDL, the model is based on the Pseudo Partial Derivative (PPD). For PFDL, the model is based on the Pseudo Gradient (PG). For FFDL, the model is based on the Pseudo Jacobian Matrix (PJM).

The system under consideration is characterized by the following: 1) SISO system, 2) hard to obtain mathematical model, 3) nonlinear I/O relationship, and 4) the reference active power flow is a fast dynamic time varying signal since the consumption needs from grid and EES system are dynamic. It appears that the CFDL control method is the best fit theoretically. CFDL has the shortest response time when the input is rapidly changing since PPD is based

on the I/O data from the last 2 iterations. Under certain practical assumptions, the monotonic convergence and bounded-input bounded-output (BIBO) stability of the CFDL data model based MFAC can be guaranteed. Thus, for the implementation of CFDL controller into the DAB converter control loop, the structure is shown in Fig. 3.3.

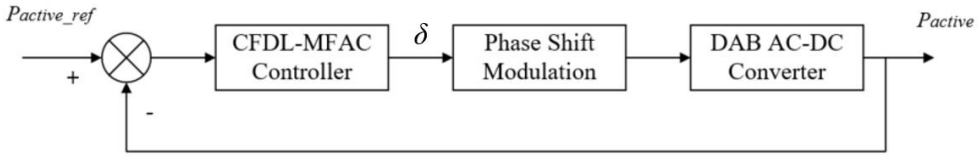

Fig. 3.3 DAB Closed Control Loop with CFDL-MFAC Controller

3.3.2 Methodology of CFDL

In this section we introduce the methodology of CFDL applied to the target system.

Consider a class of SISO nonlinear discrete-time systems described by

$$y(k+1) = f\left(y(k),...,y(k-n_y),u(k),...,u(k-n_u)\right), \tag{3.2}$$

where $u(k) \in R$ and $y(k) \in R$ are the control input and the system output at time instant *k*, respectively, The parameters n_y and n_u are two unknown positive integers, and $f : R^{n_u+n_y+2} \to R$ is an unknown nonlinear function.

A lot of nonlinear system models, such as the Hammerstein model, the bilinear model, can be shown to be the special cases of the model described by equation 3.2 which has been proved in [12]. Some assumptions are made based on system (3.2) before the CFDL method is elaborated.

Assumption 1

The partial derivative of $f(\bullet)$ with respect to the (n_y+2)th variable is continuous, for all *k* with finite exceptions.

Assumption 2

System (3.2) satisfies the generalized Lipschitz condition, for all k and $0 < b < \infty$ with finite exceptions,

$$\left| y\left(k_1 + 1\right) - y\left(k_2 + 1\right) \right| \le b \left| u\left(k_1\right) - u\left(k_2\right) \right|, \tag{3.3}$$

And for $u\left(k_1\right) \ne u\left(k_2\right)$ and $k_1 \ne k_2, k_1, k_2 \ge 0$, where

$y\left(k_i + 1\right) = f\left(y\left(k_i\right), ..., y\left(k_i - n_y\right), u\left(k_i\right), ..., u\left(k_i - n_u\right)\right), i = 1, 2$.

From a practical point of view, these assumptions imposed on the plant are reasonable and acceptable. Assumption 1 is a typical constraint for general nonlinear systems in the field of control system design. Assumption 2 imposes an upper bound on the change rate of the system output driven by the change of the control input. From an energy viewpoint, the energy change inside a system cannot go to infinity if the energy change of the control input is at a finite level. Many practical systems satisfy this assumption, such as temperature control systems, pressure control systems, liquid level control systems.

To facilitate the following theorem, define $\Delta y\left(k + 1\right) = y\left(k + 1\right) - y\left(k\right)$ as the output change and $\Delta u\left(k\right) = u\left(k\right) - u\left(k - 1\right)$ as the input change between two consecutive instants.

Theorem

Consider nonlinear system (3.2) satisfying assumptions 1 and 2. If $\left|\Delta u\left(k\right)\right| \ne 0$, then there exists a time-varying parameter $\phi_c\left(k\right) \in R$, call the Pseudo Partial Derivative (PPD), such that system (3.2) can be transformed into the following CFDL data model:

$$\Delta y\left(k + 1\right) = \phi_c\left(k\right) \Delta u\left(k\right), \tag{3.4}$$

which could also be expressed as following：

$$y\left(k + 1\right) = y\left(k\right) + \phi_c\left(k\right) \Delta u\left(k\right), \tag{3.5}$$

and with bounded $\phi_c(k)$ for any time *k*.

Equation 3.5 is a virtual equivalent dynamic linearization description of nonlinear system (3.2). It is a controller-design-oriented linear time-varying data model with a scalar parameter and in a simple incremental form. In this sense, it is totally different from the other linearized models derived from the first principles and the other linearization methods.

For a discrete-time system, the controller algorithm obtained from one-step-ahead prediction error cost function may yield excessive control effort, which might damage the control system, whereas the controller algorithm obtained from weighted one-step-ahead prediction error cost function may lead to constant tracking error. Thus, this design uses the following quadratic cost function of controller input to design the controller algorithm,

$$J(u(k)) = \left|y^*(k+1) - y(k+1)\right|^2 + \lambda \left|u(k) - u(k-1)\right|^2, \tag{3.6}$$

where $\lambda > 0$ is a weighting factor introduced to restrict the changing rate of the control input. The parameter $y^*(k+1)$ is the desired reference output signal.

Substituting CFDL data model 3.5 into cost function 3.6, differentiating cost function 3.6 with respect to $u(k)$, and setting it to zero, yields the following control law:

$$u(k) = u(k-1) + \frac{\rho \phi_c(k)}{\lambda + \left|\phi_c(k)\right|^2}\left(y^*(k+1) - y(k)\right), \tag{3.7}$$

where the step factor $\rho \in (0,1]$ is added to generalize the controller algorithm.

The theorem shows that nonlinear system (3.2), satisfying assumptions 1 and 2, can be described by dynamic linearization data model 3.3 with a time-varying PPD parameter $\phi_c(k)$. Controller algorithm 3.7 can be used only if PPD is known. The accurate value of PPD, nevertheless, is difficult to obtain since the mathematical model of the system is

unknown and PPD is a time-varying parameter. Therefore, it is necessary to design a certain time-varying parameter estimation algorithm using the I/O data of the controlled plant to estimate PPD online.

The common cost function of the time-varying parameter estimation is to minimize the square of the error between real system output and model output. By applying the estimation algorithm derived from this kind of cost function, however, the estimated value of the parameter is often sensitive to some inexact sampling data, which may be caused by disturbance or a faulty sensor. To overcome this drawback, a new cost function of PPD estimation is proposed as follows:

$$J\left(\phi_c\left(k\right)\right)=\left|y\left(k\right)-y\left(k-1\right)-\phi_c\left(k\right)\Delta u\left(k-1\right)\right|^2+\mu\left|\phi_c\left(k\right)-\hat{\phi}_c\left(k-1\right)\right|^2, \tag{3.8}$$

where $\mu>0$ is a weighting factor.

Minimizing cost function 3.6 with respect to $\phi_c\left(k\right)$ give the following PPD estimation algorithm:

$$\hat{\phi}_c\left(k\right)=\hat{\phi}_c\left(k-1\right)+\frac{\eta\Delta u\left(k-1\right)}{\mu+\Delta u\left(k-1\right)^2}\left(\Delta y\left(k\right)-\hat{\phi}_c\left(k-1\right)\Delta u\left(k-1\right)\right), \tag{3.9}$$

Where the step factor $\eta\in\left(0,2\right]$ is added to make the algorithm 3.7 more general and more flexible, and $\phi_c\left(k-1\right)$ denotes the estimation of $\phi_c\left(k\right)$.

By integrating controller algorithm 3.7 and parameter estimation algorithm 3.9, the CFDL–MFAC scheme is constructed as follows:

$$\hat{\phi}_c\left(k\right)=\hat{\phi}_c\left(k-1\right)+\frac{\eta\Delta u\left(k-1\right)}{\mu+\Delta u\left(k-1\right)^2}\left(\Delta y\left(k\right)-\hat{\phi}_c\left(k-1\right)\Delta u\left(k-1\right)\right), \tag{3.10}$$

$$\hat{\phi}_c\left(k\right)=\hat{\phi}_c\left(1\right),\ \text{if}\ \left|\hat{\phi}_c\left(k\right)\right|\le\xi\ \ \text{or}\ \ \left|\Delta\left(u-1\right)\right|\le\xi,\ \text{or}\ \ sign\left(\hat{\phi}_c\left(k\right)\right)\ne sign\left(\hat{\phi}_c\left(1\right)\right),$$

$$u(k)=u(k-1)+\frac{\rho\hat{\phi}_c(k)}{\lambda+\left|\hat{\phi}_c(k)\right|^2}\left(y^*(k+1)-y(k)\right), \tag{3.11}$$

where ξ is a small positive constant. And $\phi_c(1)$ is the initial value of $\phi_c(k)$. By using those two equations, in every iteration, CFDL-MFAC generates the current PPD by using the PPD estimation equation, then generate the new control variable by employing the control law. The process flow of CFDL-MFAC is shown in Fig. 3.4.

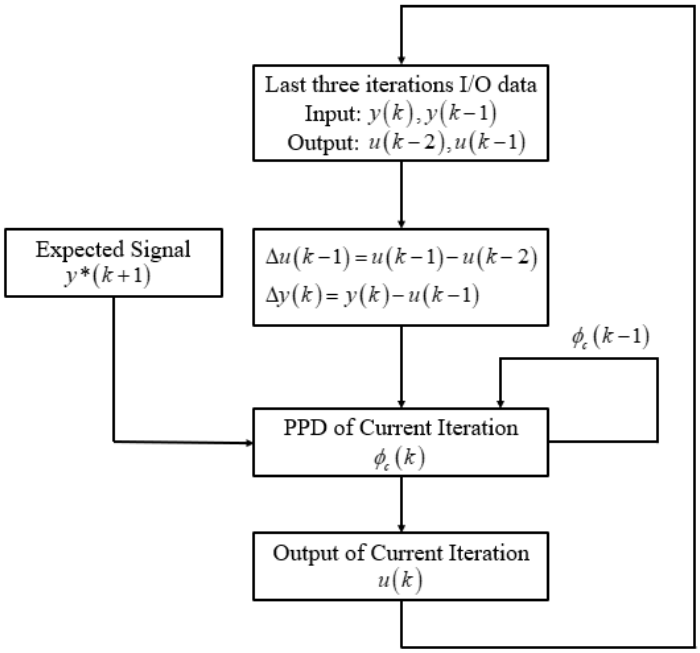

Fig. 3.4 Process of CFDL-MFAC

3.3.3 Application Analysis

From the system control scheme, there are two main factors that will greatly influence the performance of CFDL-MFAC: 1) The weighting parameters within the equation of control law and PPD estimation algorithm and 2) the initial conditions of input, output and PPD. Those two factors not only are determined by various application situations, but also influence each other. Finding proper values for those two factors based the application to improve the efficiency of MFAC is a significant part of MFAC implementation.

3.3.3.1 Weighting Parameters

In the control law and PDD estimation equation, there are four different weighting parameters within equations 3.10 and 3.11 including λ, μ, ρ, η. Their values vary from different system constraints, such as range of the input, and will greatly impact the efficiency, tracking ability, stability and convergence speed of the control system. In [25], a few laws related to choosing proper weighting parameters are introduced.

The parameter λ, it is the weighting factor for the control law, introduced to restrict the changing rate of the control input, $\Delta u(k)$. It is usually greater than 0. In general, the smaller λ is, the faster the control system responds, but the overshoot may be larger, and stability of the system is more vulnerable to damage. For most nonlinear systems, the control systems are divergent when λ is zero. Conversely, the larger λ is, the slower the control system responds, but the overshoot will be smaller, stability and robustness will be better. Parameter ρ is the step factor for control law and is added to generalize the controller algorithm. It is usually in the range of $\rho \in (0,1]$, and its relationship with λ is shown in equation 3.12.

$$\lambda > \frac{(\rho b)^2}{4} \tag{3.12}$$

where $0 < b < \infty$.

Parameters μ and η are weighting factor and step factor respectively for the PDD estimation equation, respectively. They have the similar function with λ and ρ, the name, function and value range of those parameter is shown in TABLE I.

TABLE I: Parameters in MFAC Controller

Parameters	Function	Value Range
λ	Weighting Factor of Control Law	$(0, \infty)$
ρ	Step Factor of Control Law	(0, 1]
μ	Weighting Factor of PPD Estimation Equation	$(0, \infty)$
η	Step Factor of PPD Estimation Equation	(0, 2]

3.3.3.2 Variable Initials

For the initial conditions of input, output and PPD, since MFAC is a data-driven control method, initial conditions play a very important role at the beginning of performance. Since PPD and $u(k)$ are obtained from the last iteration, for the very first iteration, there is not reference data to motivate the algorithm, so the initial conditions for the first two iteration need to be provided as a start. Under this circumstance, if the initial conditions are proper, the efficiency of MFAC will be improved greatly, especially the response time. Also, since MFAC is not a global optimization algorithm, sometimes the process will be stuck at a locally optimal solution. Proper choice of initial parameterization could reduce the probability of locally optimal solutions.

What's more, the choice of initial conditions also greatly impacts the value of the weighting parameters. For example, if the initial conditions are not proper, the input of next iteration will have a huge difference with the reference value. The step of the iteration then tends to be large, which requires the step factor to be large. However, if the step factor is large, when the response is steady, the accuracy of tracking will be reduced, even a small difference will result in a large change on the output and vice versa. To achieve better performance of MFAC, choice of the initial conditions needs to be considered carefully.

3.3.4 Robustness and Disturbance Rejection MFAC

The stability of CFDL have been proved in [26]. This paper contains a theoretical analysis of the bounded-input bounded-output stability, the monotonic convergence of the tracking error dynamics, and the internal stability of the full form dynamic linearization based MFAC scheme, which demonstrates that CFDL-MFAC is stable in most applications. The robustness of the traditional model-based control method is dynamically defined according to uncertainty or unmodeled. Since the design of the controller of the MFAC algorithm does not include the model information of any controlled system, the robustness based on model uncertainty is not relevant in the MFAC theory. The authors in [27] pointed out that the robustness of this type of model-free control method, also known as the data-driven control method, should be based on what kind of data loss level and data noise disturbance the system performance can contend with such as stability and convergence can still be maintained.

In [12], simulations show that when no measurement disturbance exists in the system, the error of output could converge to zero. However, when there is measurement disturbance, the error of output converges to a constant yielding measurable disturbance impacts on the convergence and performance of MFAC. Therefore, to improve the working performance, certain disturbance rejection methods are needed.

In [28], a disturbance suppression algorithm with filtering based on CFDL is proposed to decrease the impact on performance caused by disturbance. The key method of this algorithm is adding an extra filter on the error signal which stands for the difference between the input signal and reference signal yielding a modification based on the control law of equation 3.11. The modified control law and error signal is shown in equation 3.13 and 3.14.

$$u(k)=u(k-1)+\frac{\rho\hat{\phi}_c(k)}{\lambda+\left|\hat{\phi}_c(k)\right|^2}z(k), \tag{3.13}$$

$$z(k)=L(q)e(k), \tag{3.14}$$

where $L(q)$ is a linear filter, and $z(q)$ is the filtered signal of error signal $e(k)$. The theoretical analysis of its functionality could also be found in [28].

Then the key point of implementing the disturbance suppression MFAC algorithm with filtering is designing a proper filter for $L(q)$. Also note that the disturbance/noise signal in real-world usually contains high-frequency content, so the filter is typically designed as low-pass filter. More simulations and discussion over this improved algorithm will be presented in chapter 4.

Chapter 4: Simulation Validation and Comparison

4.1 Simulation Conditions

4.1.1 Converter Parameters

For the simulation of single-stage DAB AC/DC converter, the Simulink model is shown in Fig. 4.1. The parameters of each component are shown in TABLE II. Note that the switches within the model are realized by using IGBT transistors.

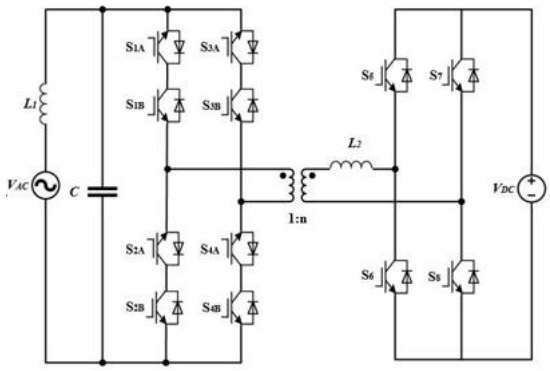

Fig. 4.1 Model of Single-Stage DAB AC/DC Converter

TABLE II: Parameters of the Converter

Parameters	Function	Value
n_t	Turn ratio of transformer	1
V_{ac}	RMS value of the AC source voltage	100V
V_{dc}	Value of the DC source voltage	250V
L_2	Leakage inductance of the transformer	50uH
f_i	Frequency of the AC source	60Hz
f_s	Switching frequency of the switches	20kHz
C	Capacity of the LC filter circuit on AC side	15uF
L_1	Inductance of the LC filter circuit on AC side	0.9mH
d_{ac}	Duty cycle on the primary side	50%
d_{dc}	Duty cycle on the secondary side	40%
δ	Phase shift ratio	[-0.5, 0.5]

According to equation 2.7 in chapter 2, there is a linear relationship between d_{dc} and δ. If the value d_{dc} is fixed, based on selected input voltage, output voltage, and turn ratio, the

value of δ is limited by equation 2.7. Furthermore, the range of δ is decreased if d_{dc} is increased and vice versa. Based on the parameters of the converter, the calculated value of d_{dc} is 0.4. The δ is in the range of $[-0.6, 0.6]$. However, during the working process of converter, since the voltage of v_{ac} is changing, d is supposed to change with it, so in the model d_{dc} is defined by equation 2.6 and it is a dynamic parameter and in order to obtain the maximum efficiency and reasonable range of δ at same time, this design utilizes δ in the range of $[-0.6, 0.6]$, which is also shown in TABLE II.

4.1.2 PID Controller Parameters

For the PID controller, this design employed a PI controller based on the features of the target system, which has the general transfer function form that is shown in equation 4.1.

$$G(s) = \frac{k_p(s + k_i)}{s(s + p)}, \tag{4.1}$$

After some simulations, the parameters that this design use are $K_p = 0.01, K_i = 0.1,$ $p = 0.01,$ which indicates the transfer function of this PI controller is shown in equation 4.2.

$$G(s) = \frac{0.01s + 0.001}{s^2 + 0.01s}, \tag{4.2}$$

4.1.3 Evaluation Indexes

1) Loss Function

In order to evaluate the performance of a control system and make comparison among different controllers, evaluation indexes are needed during tests. For the control system, we consider performance characteristics during transient dynamics. According to the statements in [29], there are three kinds of indexes commonly used in evaluation: 1) Quality indexes for transient process, such as overshot, adjust time, rise time etc. 2) Positive Definite Quadratic

Integral Functional, which is the application of Lyapunov second method in optimal control and 3) The Error Functional Integral Evaluation Index in which deviation integral performance index uses the objective function in the form of deviation integral to evaluate the response performance of the control system. This is a direct quantitative range and can evaluate the characteristics of the entire step response transient curve. The general form is shown as below in equation 4.3.

$$I = \int_0^\infty t^n \left| e(t) \right|^m dt, \tag{4.3}$$

where the error is defined as $e(t) = y_{\text{ref}} - y(t)$, and it is a function over time. The parameter y_{ref} is the reference signal. When $n = 1$ and $m = 1$, this evaluation index could be defined as Integral of Time Multiply by Absolute Error Index (ITAE). Its essence is to weight the deviation integral area with time, which is often used for parameter tuning of control system. ITAE performance can directly reflect the control performance of the system, so this design takes ITAE as the loss function. And during the testing, since the switching frequency is relatively high with respect to the controller frequency, the sampling time for ITAE is super small, which leads to huge numerical value of ITAE, so this design made certain numerically modification on the original ITAE, to generalize this index. Also, in order to decrease the unreasonable factor in the evaluation, this design starts to calculate ITAE at *0.1s* after the system begins to run. The final form of ITAE that is used in this design is shown in 4.4.

$$I = \frac{\sum_{0.1}^{\infty} t \left| e(t) \right|}{10^6}, \tag{4.4}$$

For this index, loss function, the smaller the value is, the closer the output signal value with the reference signal value as a whole, which indicates good performance of this controller.

2) Rise Time

The index of rise time refers the amount of time from $t = 0$, to the point when the control system entering steady state. As for the definition of entering steady state, this design stipulates that if the error between the output and reference signal is less than 5% of the reference signal value in ten continuous iterations, we consider the control system has entered steady state, and the time of the last iteration during that period is considered as the rise time. This indicates the response ability of a control system. A process diagram is shown in Fig. 4.2.

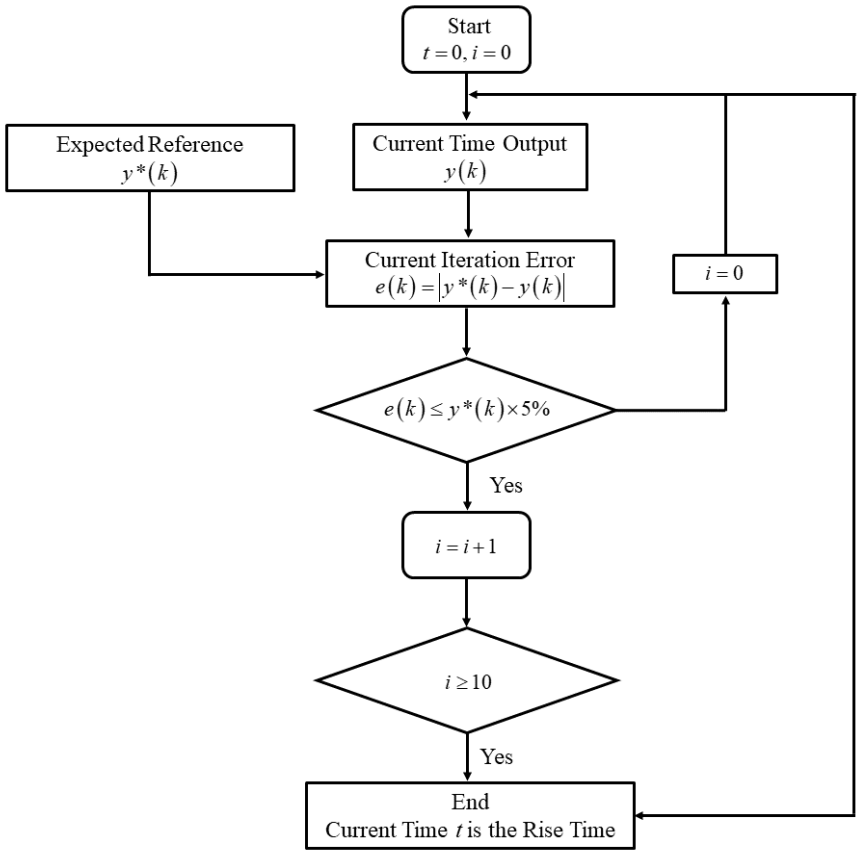

Fig. 4.2 Process of Defining Rise Time

For this index, rise time, the smaller the value, the faster this control system responds to the change of input signal, which indicates good response for this controller.

4.2 Simulation on Single-Stage DAB AC/DC Converter under SHBM

Based on the model of single-stage DAB AC/DC converter shown in Fig. 4.1, this design employed the Simulink model of the DAB AC/DC converter under SHBM that is presented in appendix A. Simulations over the functionality of this converter model with SHBM are performed in this session. In the first simulation, $d_{dc} = 40\%, \delta = 0.1$, and waveforms of the primary voltage v_p, secondary voltage v_s, leakage inductor voltage v_L and current i_L and active power flow are shown in Fig. 4.3, respectively.

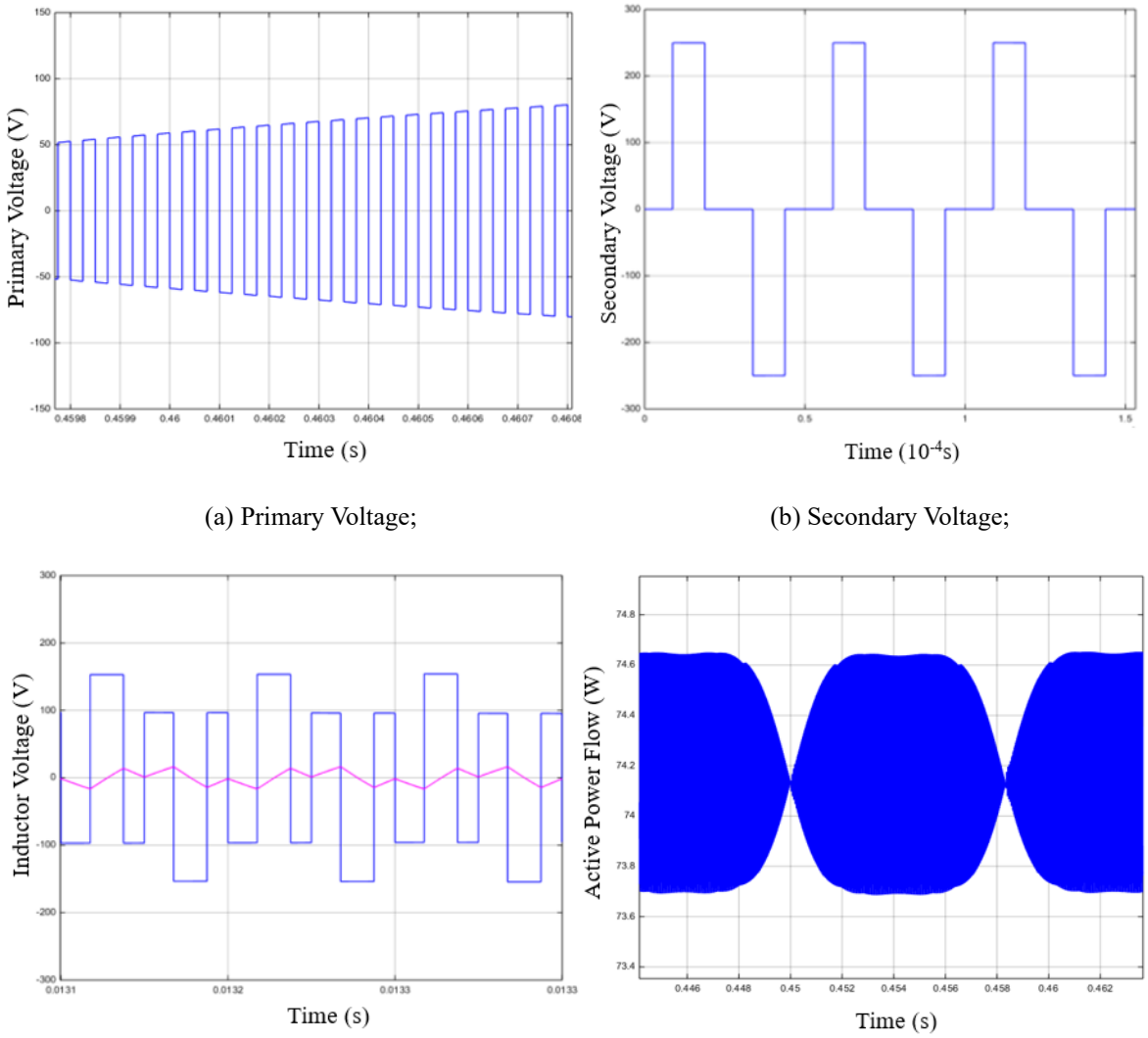

(a) Primary Voltage; (b) Secondary Voltage;

(c) Inductor Voltage (Blue) and Current (Red, A); (d) Active Power Flow;

Fig. 4.3 Waveforms of $d_{dc} = 40\%, \delta = 0.1$.

As for the second simulation, $d_{dc} = 40\%, \delta = 0.3$, the result waveforms are shown in Fig. 4.4. And for third simulation, $d_{dc} = 40\%, \delta = -0.3$, the result waveforms are shown in Fig. 4.5 as below.

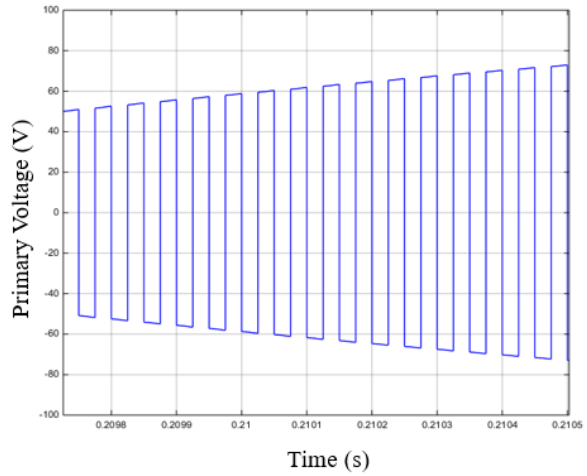

(a) Primary Voltage;

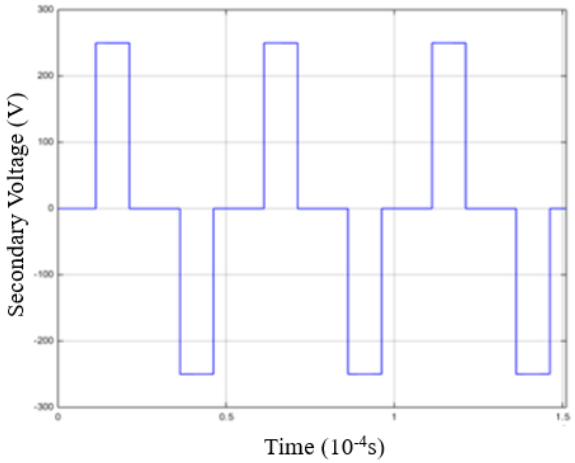

(b) Secondary Voltage;

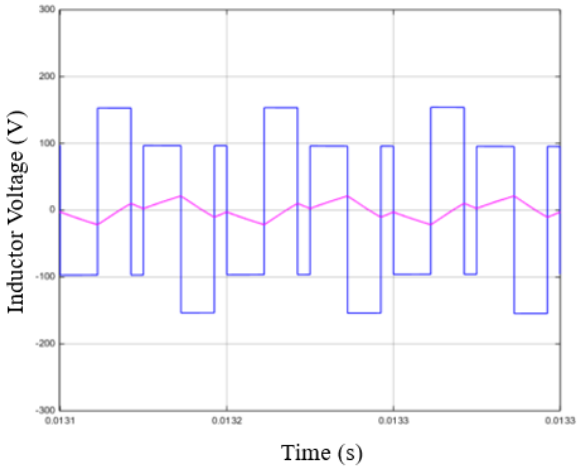

(c) Inductor Voltage (Blue) and Current (Red, A);

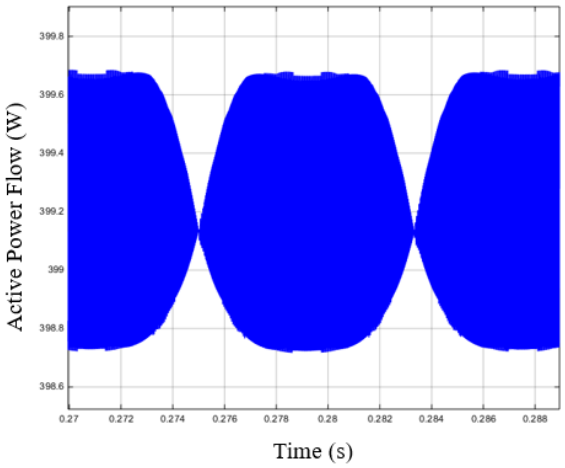

(d) Active Power Flow;

Fig. 4.4 Waveforms of $d_{dc} = 40\%, \delta = 0.3$.

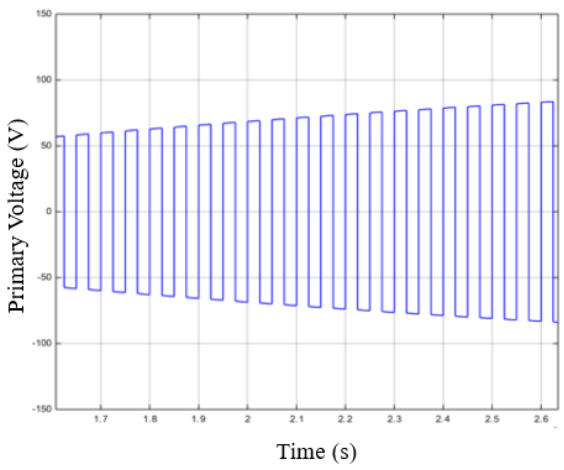

(a) Primary Voltage;

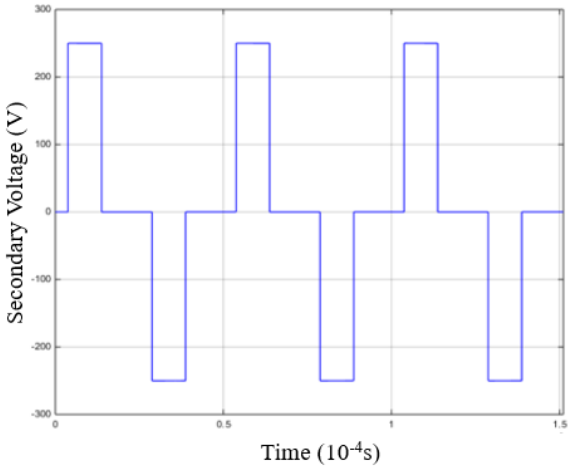

(b) Secondary Voltage;

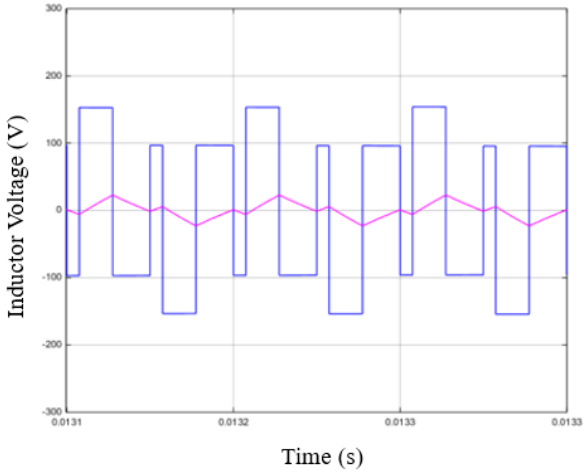

(c) Inductor Voltage (Blue) and Current (Red, A);

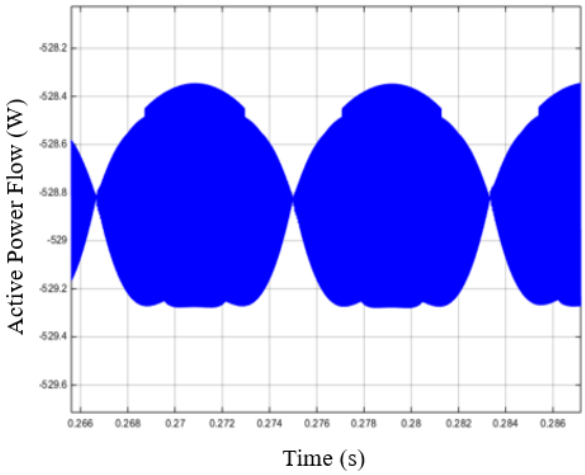

(d) Active Power Flow;

Fig. 4.5 Waveforms of $d_{dc} = 40\%, \delta = -0.3$.

Comparing Fig. 4.3 with Fig. 4.4, based on different phase shift ratio under the fixed duty cycle *d*, the waveforms of the leakage inductor voltage and current are different, which directly results in the diverse active power flow shown in Fig. 4.3 (d) and Fig. 4.4 (d). Those two simulations not only prove that the converter model is functional, but also prove that, under SHBM, the phase shift ratio will have direct impact on the inductor current which leads to influence on the active power flow. Comparing Fig.4.4 with Fig. 4.5, based on the phase shift ratio with same value and opposite sign under the fixed duty cycle *d*, the change on the

leakage inductor voltage and current leads to negative active power flow shown in Fig. 4.5 (d), which indicates that power flow is from the ESS to the power grid and proves that DAB AC/DC converter has the ability to convert energy bi-directionally. Those three simulations validate the functionality of the Simulink converter model, which allows the following simulation to perform based on this model.

4.3 Simulation on PID Control

According to the control scheme discussed in chapter 3 and PID controller designed in session 4.1.2, the Simulink model of the PID control scheme is built and shown in Appendix B. The following simulations are performed to validate and explore the PID control system.

1) Functionality of PID Control System

In this simulation, the reference signal of active power will be two constant signals, 350W and -350 W, respectively. By observing output active power flow of the converter, the functionality of PID control system could be validated and values of the two evaluation indexes utilized, ITAE and rise time, could be obtained. The results are shown in Fig. 4.6 and Fig. 4.7.

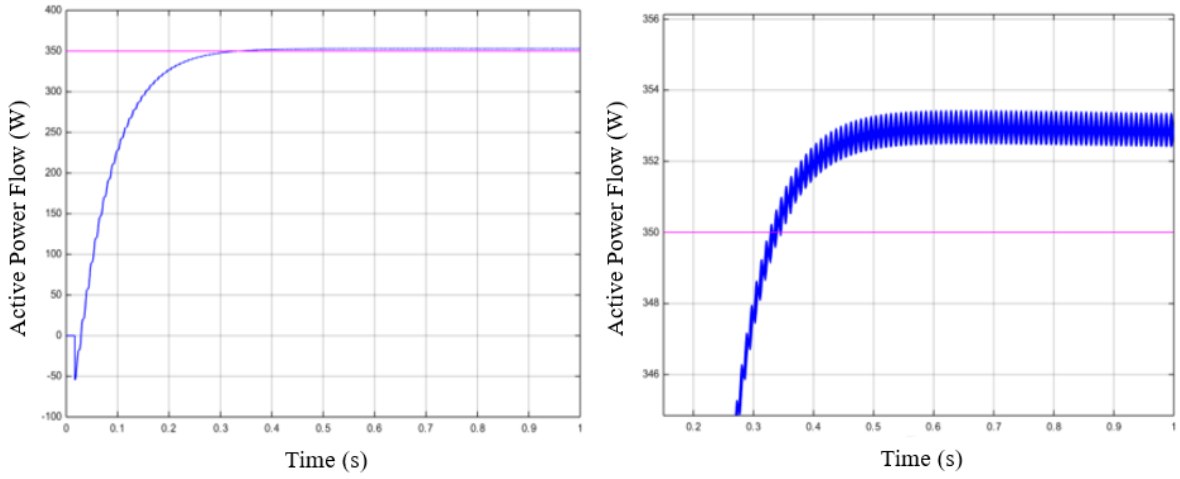

(a) Active Power Flow (Blue) and Reference Power Flow (Red);

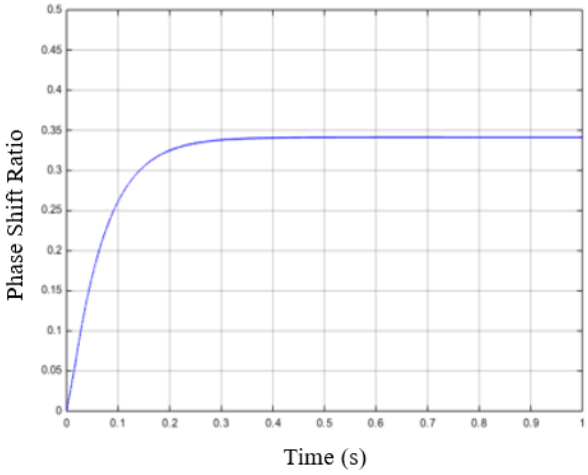

(b) Waveform of Phase Shift Ratio;

Fig. 4.6 Waveforms of PID Controller, $P_{active} = 350\text{W}$.

In this test, ITAE is 3.101, and rise time is 0.2708s. The active power value is around 353W in the stable stage and the phase shift ratio is around 0.34.

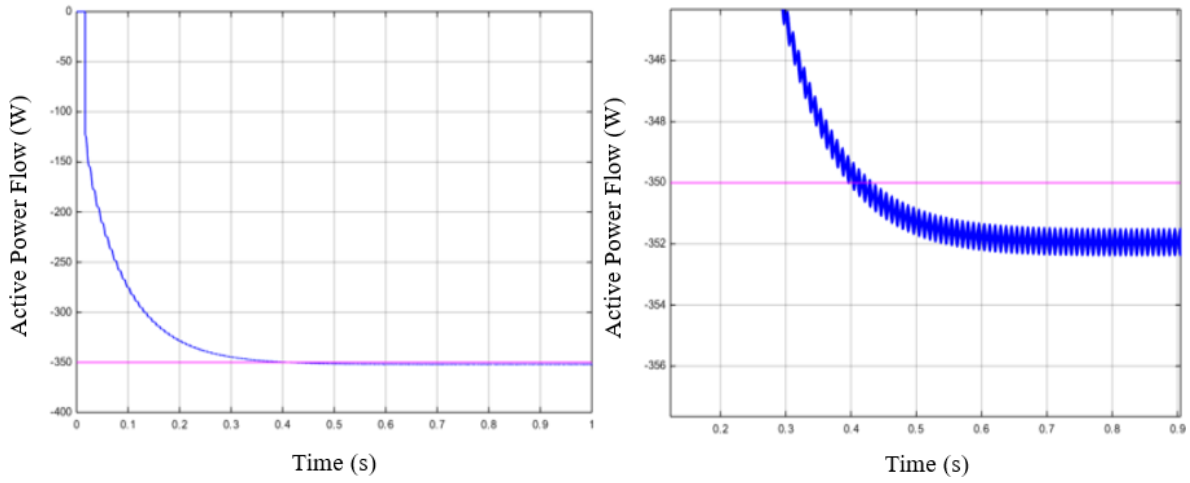

(a) Active Power Flow (Blue) and Reference Power Flow (Red);

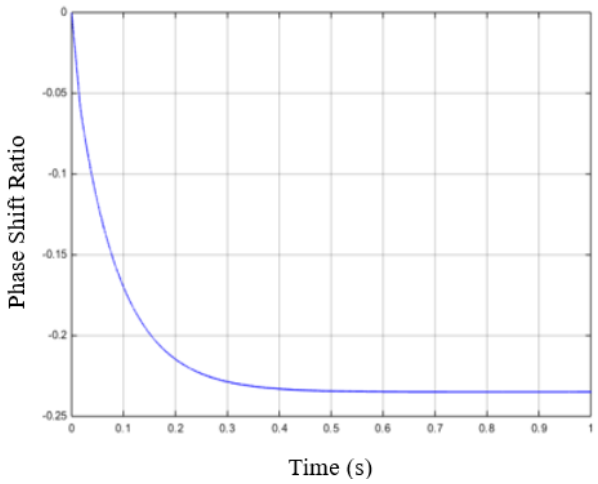

(b) Waveform of Phase Shift Ratio;

Fig. 4.7 Waveforms of PID Controller, $P_{\text{active}} = -350\text{W}$.

In this test, ITAE is 4.396, and rise time is 0.3025s. The active power value is around -352W in the stable stage and the phase shift ratio is around -0.235. Comparing those two simulations, the results show that PID controller could control bi-directional power flow of converter. Although the stable power flow value is close to the reference value, the rise time is relatively large. Since the input are constant signals in this simulation, the tracking ability of PID controller needs to be further tested.

2) Influence of the Duty Cycle and Phase Shift Range on PID Control System

Duty cycle d_{dc} and the range of δ are two important factors that influent the performance of the converter. To evaluate their impact on the PID control system, two controlled simulations are performed with $P_{\text{active}} = 350\text{W}$. In the first test, instead of using dynamic d_{dc}, a constant, 0.4, is utilized, and the range of δ remains from 0.5 to -0.5. The result is shown in Fig. 4.8.

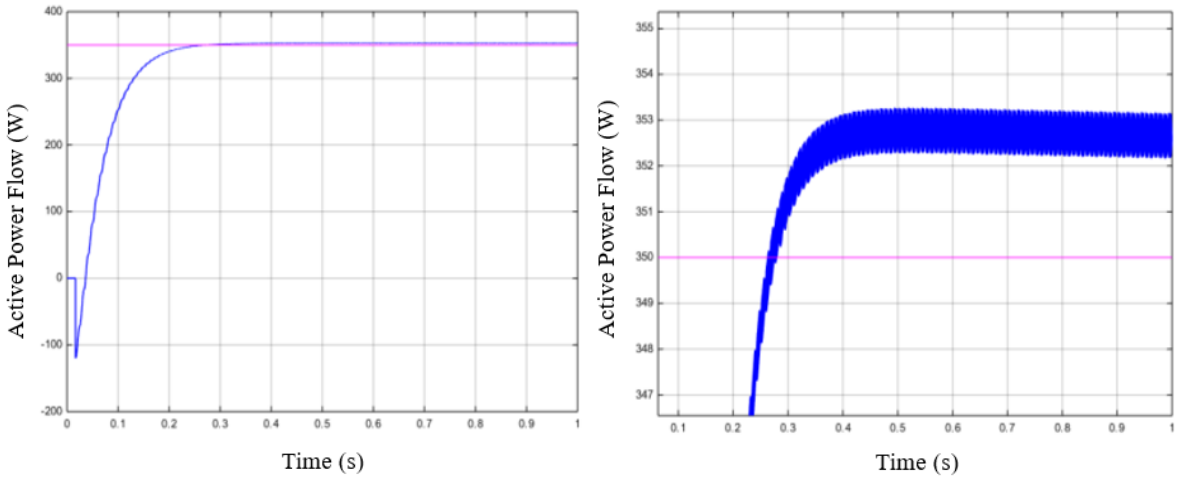

(a) Active Power Flow (Blue) and Reference Power Flow (Red);

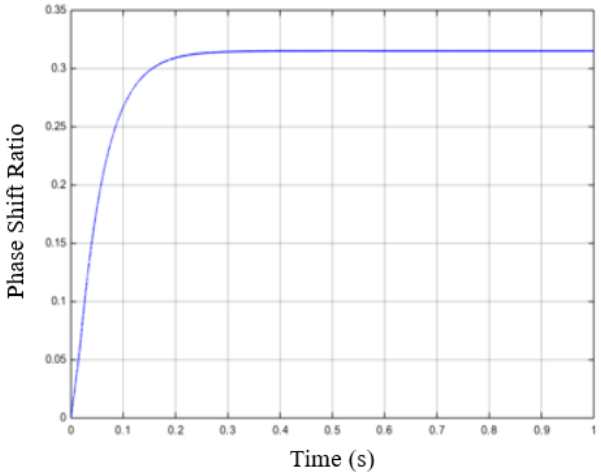

(b) Waveform of Phase Shift Ratio;

Fig. 4.8 Waveforms of PID Controller, $d_{dc} = 0.4$.

In this test, ITAE is 2.431, and rise time is 0.2208s. The active power value is around 352.5W in the stable stage and the phase shift ratio is around 0.315. Compared to the result in (a), rise time becomes shorter, stable stage power value is almost the same, and the phase shift ratio is different, which indicates the performance of PID controller system is better when duty cycle remains as a constant. However, in real-world, the d_{dc} changes with AC-side periodic voltage. Although constant duty cycle will have better control performance, in order to generalize the power flow control system, dynamic d_{dc} is utilized for the rest of tests.

In the second test, the range of δ is changed from $[-0.5, 0.5]$ to $[-0.6, 0.6]$ and $[-0.25, 0.25]$ respectively, and the duty cycle remains dynamic. The simulation are performed to explore the influence of phase shift ration range. The test result of $[-0.25, 0.25]$ is shown in Fig. 4.9 as below.

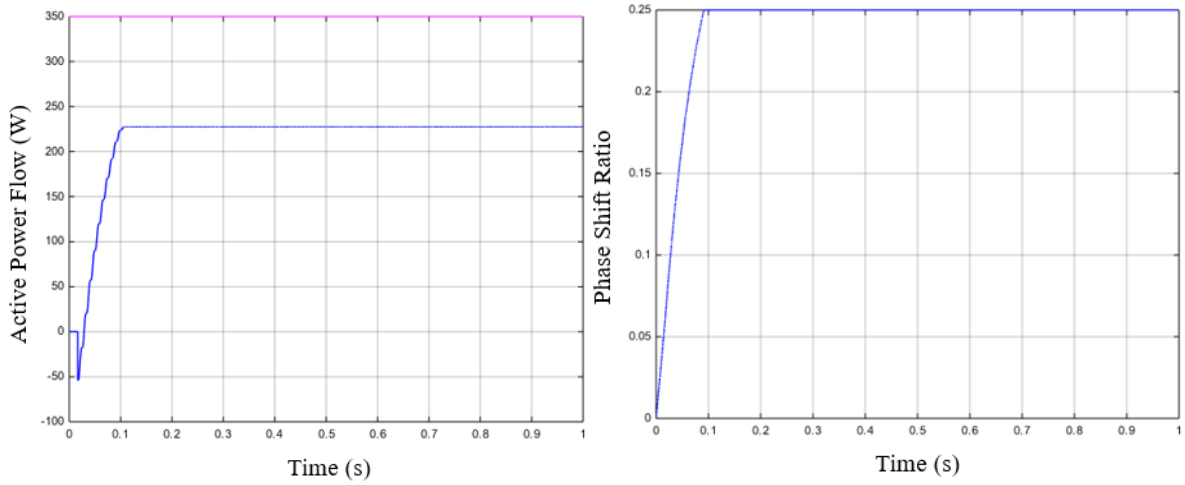

(a) Active Power Flow (Blue) and Reference Power Flow (Red); (b) Waveform of Phase Shift Ratio;

Fig. 4.9 Waveforms of PID Controller, δ is [-0.25, 0.25].

According to the result, when the range is too small, the expected δ value is out of the bounded range, the both the ITAE value and rise time will be impacted. For the test above, ITAE is 80.15, and rise time does not exist since the response value is far away from the reference value, which indicate bad performance of this control system. When the range of δ is $[-0.6, 0.6]$, the result shows that the rise time, ITAE, stable stage active power value and δ almost remain the same, which indicates that larger range of δ does not have much impact on the performance when stable stage δ value is within the range designed. In short, the range of δ is suppose to be bigger within the reasonable range.

3) Tracking Ability of PID Control System with Dynamic Reference

Tracking ability is one of the most important ability for a power flow control system since the power flow is dynamic and time varying. Generally, the ability of closely tracking changes of reference signal is appreciated. In this test, the active power flow reference is shown in Fig. 4.10 which is a signal combined by sine wave and step signal in equation 4.5. And the response results are shown in Fig. 4.11.

$$y_1(t) = 200\sin(6t),$$
$$y_2(t) = \begin{cases} 150;\ 0 \le t < 0.4 \\ -150;\ 0.4 \le t < 0.8 \\ 150;\ 0.8 \le t < 1 \end{cases} \tag{4.5}$$

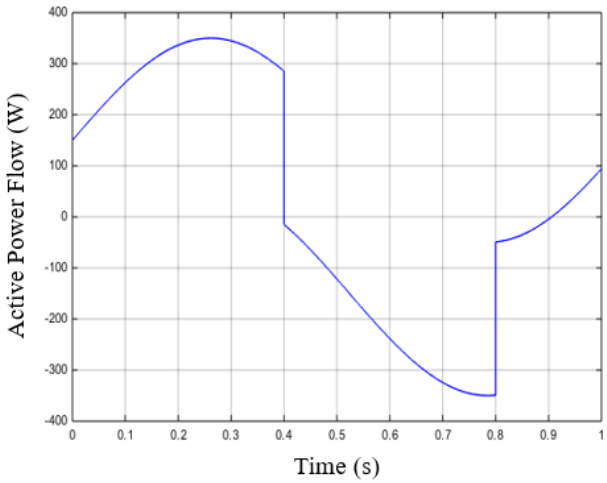

Fig. 4.10 Waveforms of Reference Active Power Flow

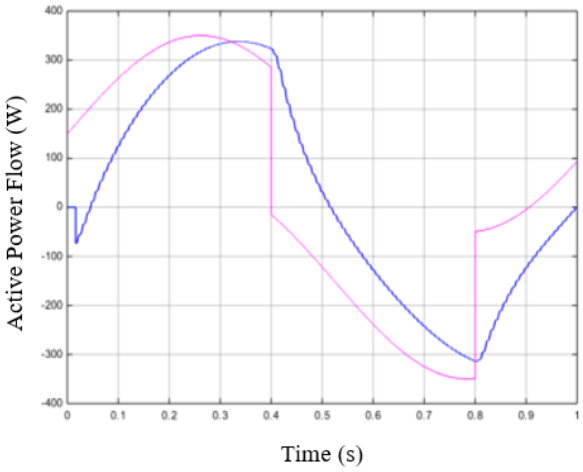

(a) Active Power Flow (Blue) and Reference Power Flow (Red);

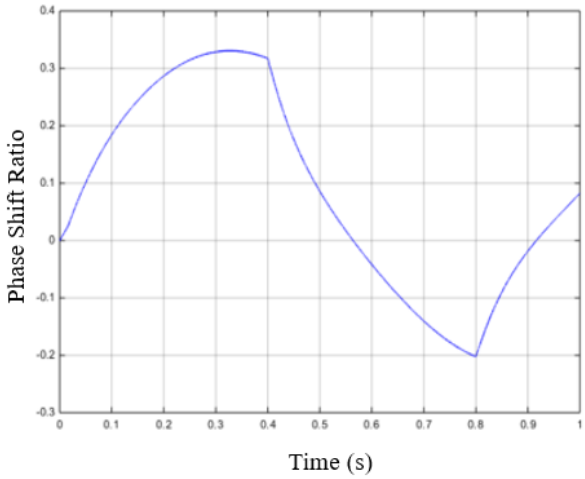

(b) Waveform of Phase Shift Ratio;

Fig. 4.11 Waveforms of PID Controller with Dynamic Reference

From Fig. 4.10 (a), the result shows that PID control system has bad tracking ability and unable to response accurately when quick changes take place on reference active power flow signal. The results indicates that PID control cannot satisfy requirements for the desired power control system, other control method need to be applied.

4.4 Simulations on MFAC

4.4.1 Benchmark Function Test

For any algorithm implementation, the first step is to verify its effectiveness. A Benchmark function is a way of evaluating the effectiveness of an algorithm. Because they represent common problems and are often used to test existing and emerging optimization algorithms. To test the CFDL-MAFC method, a benchmark function, Griewank, is utilized and its range are shown in equation 4.6.

$$f_{Gri} = \frac{1}{4000}\sum_{m=1}^{M-1} x_m^2 - \prod_{m=1}^{M}\cos\left(\frac{x_m}{\sqrt{m}}\right)+1,\ \ x\in[-600,600],\ \ f(0)=0 \qquad (4.6)$$

In this simulation, parameters of MFAC controller are: $\lambda = 0.1,\ \mu = 1,\ \rho = 0.5,\ \eta = 0.5$, also with initial conditions of inputs as $y(1) = -1,\ y(2) = 1,\ y(3) = 0.5$, outputs as $u(1) = 0,\ u(2) = 0,\ u(3) = 0$ and PPD as $fai(1) = 0,\ fai(2) = 0$. Result is shown in Fig. 4.12.

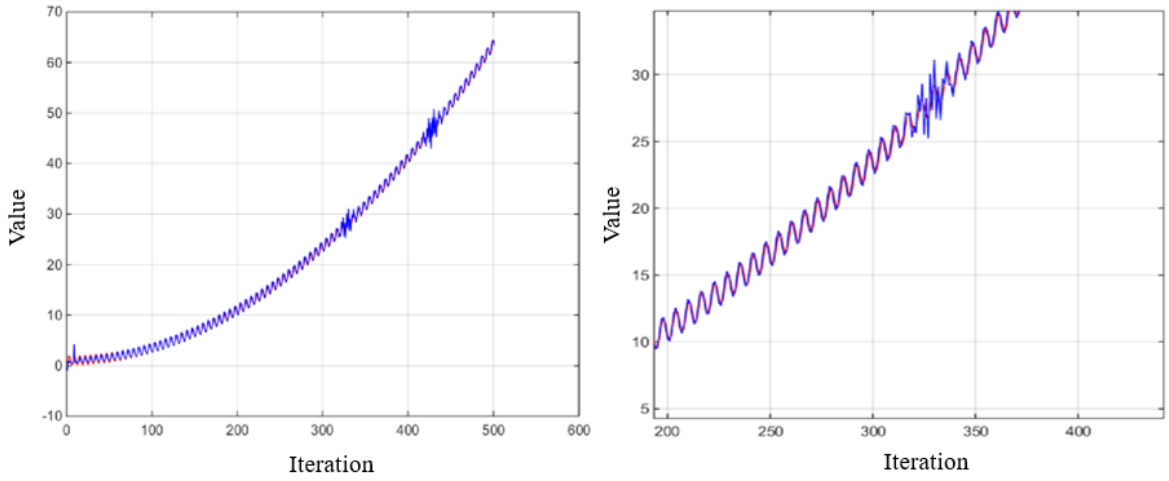

(a) Waveforms of Output (Blue) and Reference signal (Red);

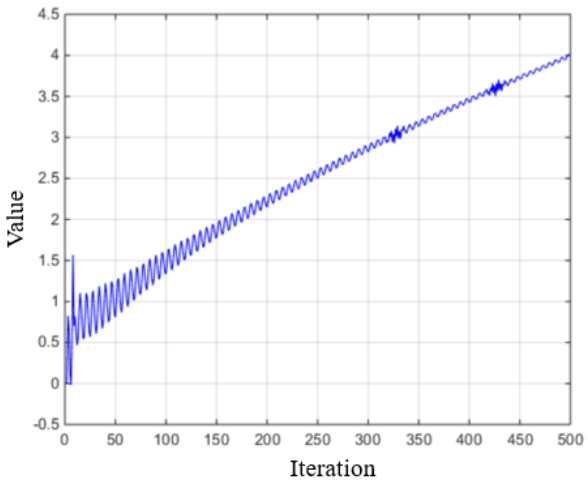

(b) Waveforms of the Input (Control Variable).

Fig. 4.12 Result of Benchmark Function Test

From the result, MFAC has great respond performance and tracking ability to the target signal, which greatly satisfies requirements for the desired power flow control system. However, further simulations are needed to explore the working performance of MFAC and validate its functionality on the DAB AC/DC converter system.

4.4.2 Parameters and Initial Conditions Test

In session 3.3.3, the impact of parameters and initial conditions on performance of MFAC has been discussed, and several general rules for tuning the parameters has also been proposed. In this part, more simulations will be performed to further validate the rules mentioned and based on which to help turn the parameters and initial conditions for the power flow control system of DAB AC/DC converter.

1) Weighting Parameters Test

For parameters λ, μ, ρ, η, one controlled simulation for each will be perform based the Griewank Benchmark function and the test in chapter 4.4.1. The results are shown in Fig. 4.13 to Fig. 4.16.

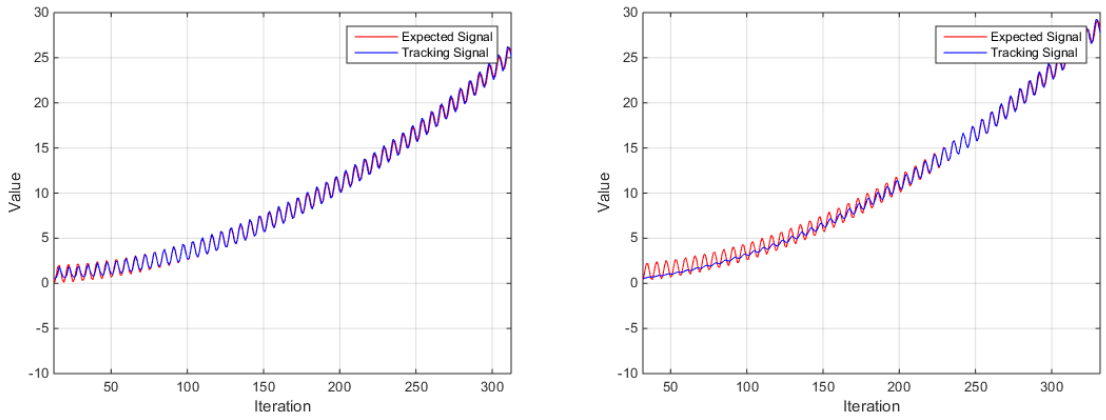

(a) $\lambda = 0.1$; (b) $\lambda = 10$.

Fig. 4.13 Result of Parameter λ Test, Weighting Parameter of Control Law

The result indicates that the bigger λ is, the slower the system coverages. As shown in Fig. 4.12 (b), at the beginning of the control process, the difference between expected and tracking signal is larger than it is in (a) and the rise time also becomes longer. In this simulation, the impact on the steady stage value is not very evident cause the waveform of

steady stage is identical, so when performing parameter tuning for MFAC system, λ is supposed to start with a small constant and gradually increased to achieve best performance.

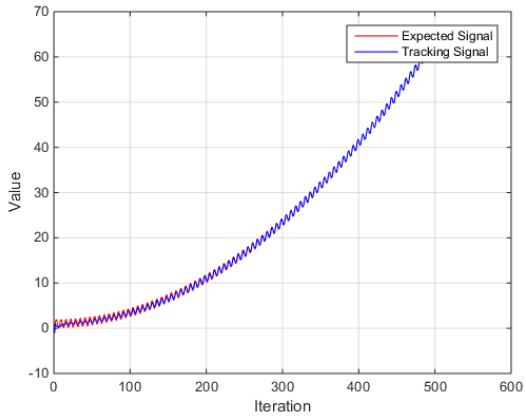

(a) $\rho = 0.1$;

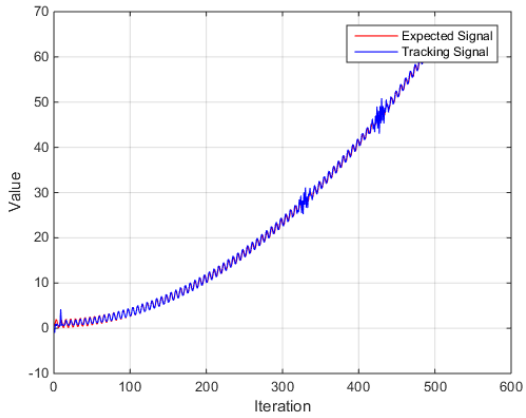

(b) $\rho = 0.5$;

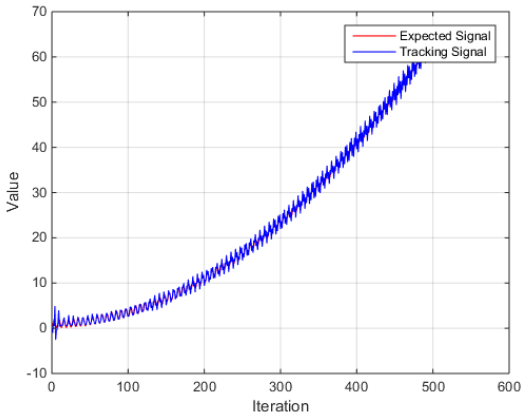

(c) $\rho = 1$.

Fig. 4.14 Result of Parameter ρ Test, Step Parameter of Control Law

The result indicates that, within the range of $(0,1]$, the smaller ρ is, the slower the system coverages, the bigger ρ is, the worst the tracking accuracy is. As shown in Fig. 4.13, the wave gets stronger and the difference gets larger in the stable stage, so ρ is supposed to start with a constant in the middle of the range when generalize to the MAFC system.

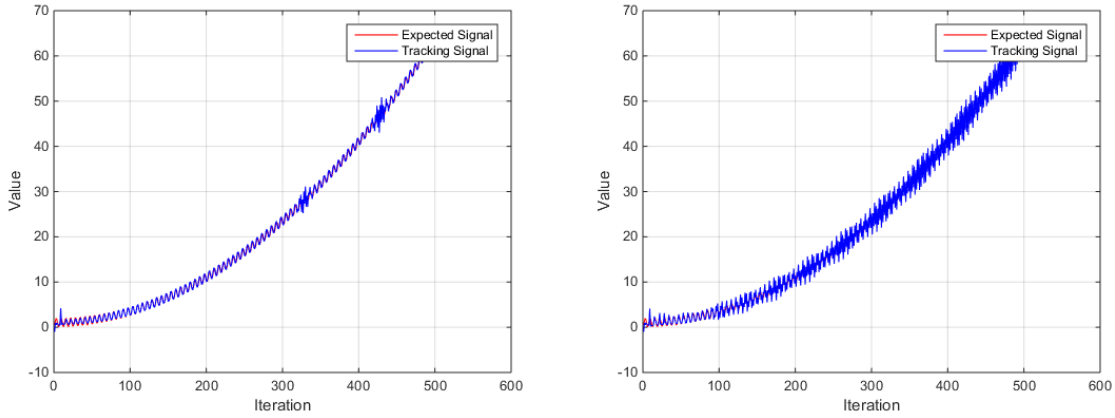

(a) μ *=1*; (b) μ *=10*.

Fig. 4.15 Result of Parameter μ Test, Weighting Parameter of PDD Estimation

The result indicates that the smaller μ is, the more stable the system is. As shown in Fig. 4.14 (b), the tracking signal is periodic waving around the expected signal, and the wave gets strong as the parameter is getting bigger. so μ is supposed to start with a small constant for MFAC system.

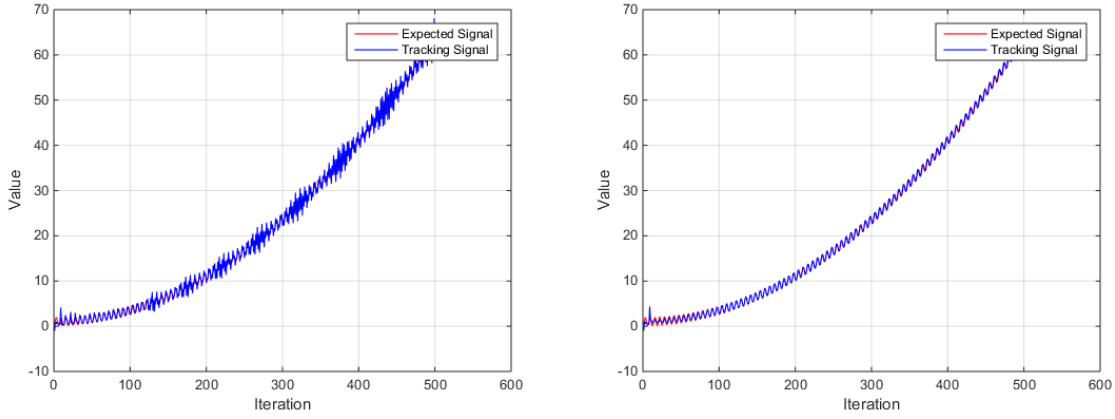

(a) η *=0.1*; (b) η *=1*.

Fig. 4.16 Result of Parameter η Test, Step Parameter of PDD Estimation

The result indicates that within the range of $(0, 2]$, the bigger η is, the more stable the system is. So η is supposed to start with a big constant within the limited range when

generalize to the MAFC system. Through the simulations above, several specific rules for parameter tuning are summarized to help find better MFAC parameters to obtain better performance.

2) Initial Conditions Test

Initial conditions have impact on the perform of MFAC system according to the methodology of CFDL-MFAC. However, the influence is different and uncertain for each system. In order to explore the influence and further improve the performance, 4 controller simulations are processed, and the initial conditions are shown in TABLE III. If we utilize k as the current iteration, then $k-1$ is the last iteration. $y(k), u(k)$, and $\phi_c(k)$ are the input, output and PDD of kth iteration. The result is shown in Fig. 4.17.

TABLE III: Initial Conditions Test Data Set

Times	Output			Input			ϕ_c	
	$y(k-3)$	$y(k-2)$	$y(k-1)$	$u(k-3)$	$u(k-2)$	$u(k-1)$	$\phi_c(k-2)$	$\phi_c(k-1)$
1	1	0.5	-1	0	0	0	2	2
2	-1	1	0.5	0	0	0	2	2
3	1	0.5	-1	1	2	3	2	2
4	1	0.5	-1	0	0	0	1	3

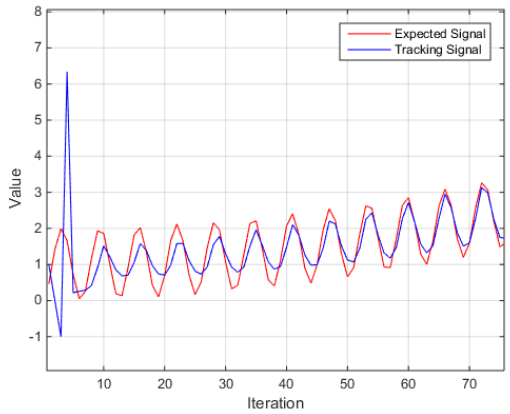

(a) Situation 1;

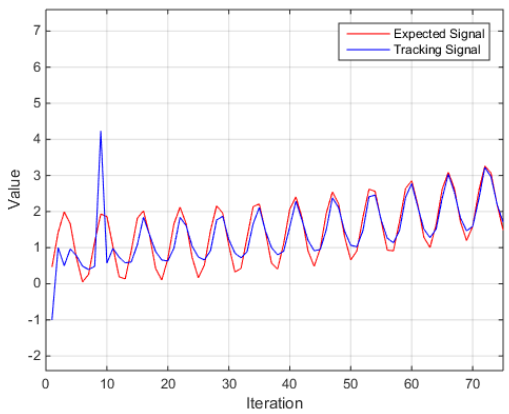

(b) Situation 2;

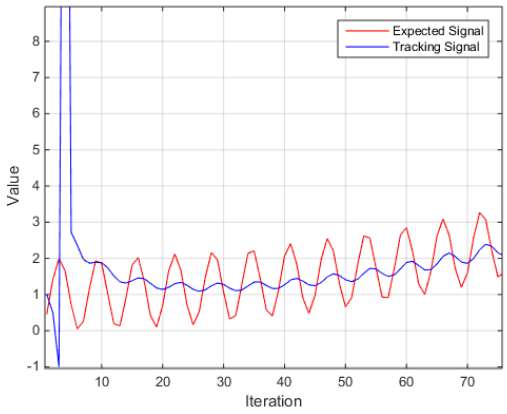

(c) Situation 3;

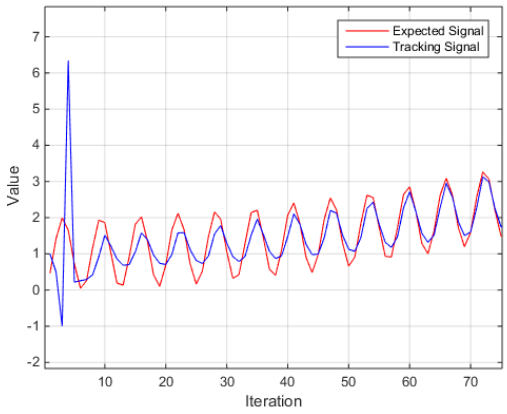

(d) Situation 4.

Fig. 4.17 Result of Initial Conditions Tests

From the four figures in Fig. 4.16, the conclusion that initial conditions will have impact at the beginning of the control process could be made. The impact usually happens within first 20 iterations out of 500 iterations, expect for output value, which has longer impact on system performance. Since for power flow control system, quick response and good stable stage performance are preferred, the impact at the first couple iteration could be overlooked. Therefore, to eliminate the impact caused by initial conditions, random values will be selected, and ITAE will be calculated after 0.1s when implementing the MFAC power flow control system.

4.4.3 Functionality Test

According to the control scheme discussed in chapter 3, the Simulink model of the CFDL-MFAC scheme is built and shown in Appendix C. The following simulations are performed to validate the functionality of CFDL-MFAC controller on the converter system.

In the first simulation, the reference signal of active power will be two constant signals, 350 and -350, respectively. The parameters are: $\lambda = 1, \mu = 1, \rho = 0.1, \eta = 1$, and the initial

conditions are inputs as $y(1)=0, y(2)=100, y(3)=200$, outputs as $u(1)=0.1, u(2)=0.1, u(3)=0.1$ and PPD as $fai(1)=2,\ fai(2)=2$. The result is shown in Fig. 4.18 and Fig. 4.19.

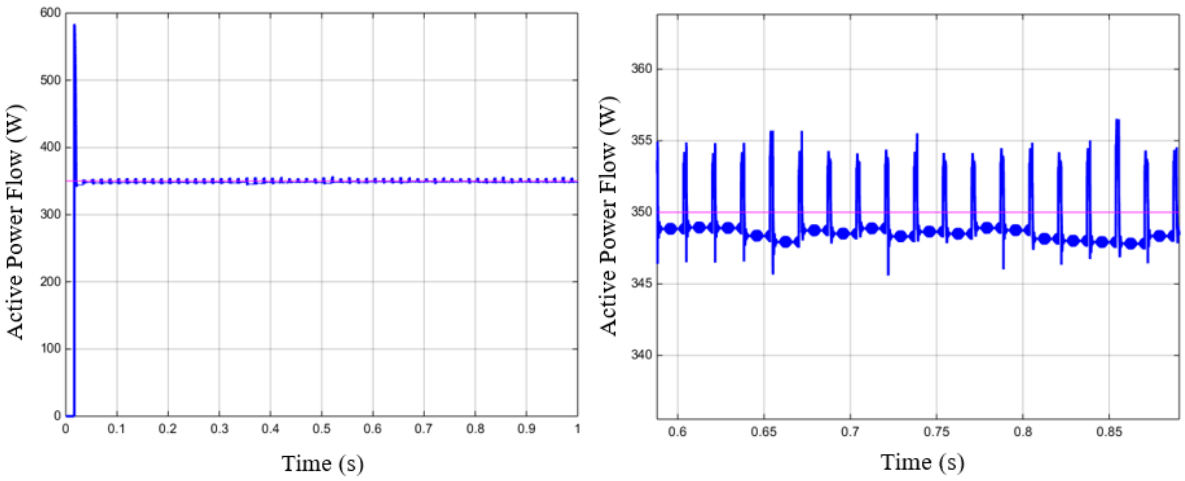

Fig. 4.18 MFAC Control System Response under 350W Reference Signal

In this test, ITAE is 1.296, and rise time is 0.0338, which is greatly reduced compared to the result of PID controller under the same test conditions. The rise time is much smaller, which indicates that MFAC system could response quick to the change from input side. However, from the second picture of Fig. 4.17, it shows that the adjustment generated by MFAC during stable stage to correspond the small change is huge, which leads to big overshot appears in the figure. This result proves the discussion in session 3.3.3 that stable stage performance could be reduced to achieve quicker response ability under fixed parameters. Therefore, the meaning of parameter tuning is fining the balance between good stable performance and quick response ability. Since the overshot is less than 0.015% and the stable stage value is around 349W, which is mostly satisfy the requirements for a good power control system, the parameters utilized in this test is accepted.

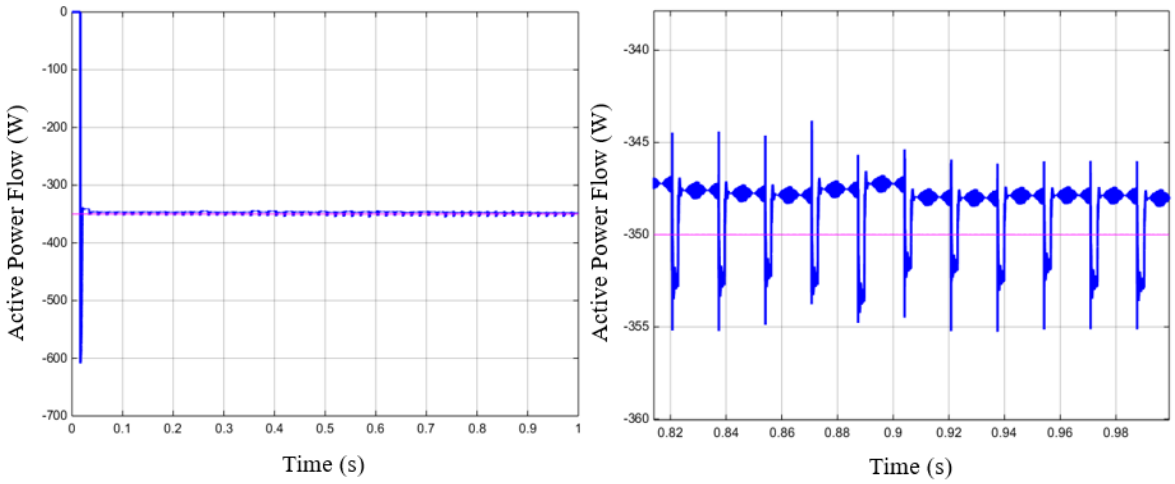

Fig. 4.19 MFAC Control System Response under -350W Reference Signal

In this test, ITAE is 2.791, and rise time is 0.0342, which is also greatly reduced compared to the PID controller under. The overshot is less than 0.015% and the stable stage value is around -348W, which also satisfy the control goal.

The initial conditions utilized in the above two simulations are randomly chosen, and the parameter values utilized are tuned according to many test results, some of the test data under $P_{\text{active\_ref}} = 350\text{W}$ are shown in TABLE IV as below, which indicates that the parameters utilized in this design is relatively optimized.

TABLE IV: Parameters Test Data Set

Times	λ	ρ	μ	η	ITAE	Rise Time (s)
1	1	0.1	1	1	1.296	0.0338
2	1	0.1	1	0.1	1.389	0.0338
3	10	0.1	1	1	2.952	0.0204
4	0.1	0.1	1	1	1.768	0.0338
5	1	1	1	1	1.598	0.0338
6	1	0.1	10	1	1.380	0.0338
7	1	0.1	0.1	1	1.828	0.0338

In the third simulation, dynamic active power flow reference signal is employed to further test the tracking ability of MFAC system. The reference signal utilized is the same as

in equation 4.5, the parameters are: $\lambda = 1, u = 1, \rho = 1, \eta = 0.1$ and the initial conditions are same as the first two simulations. The result is shown in Fig. 4.20.

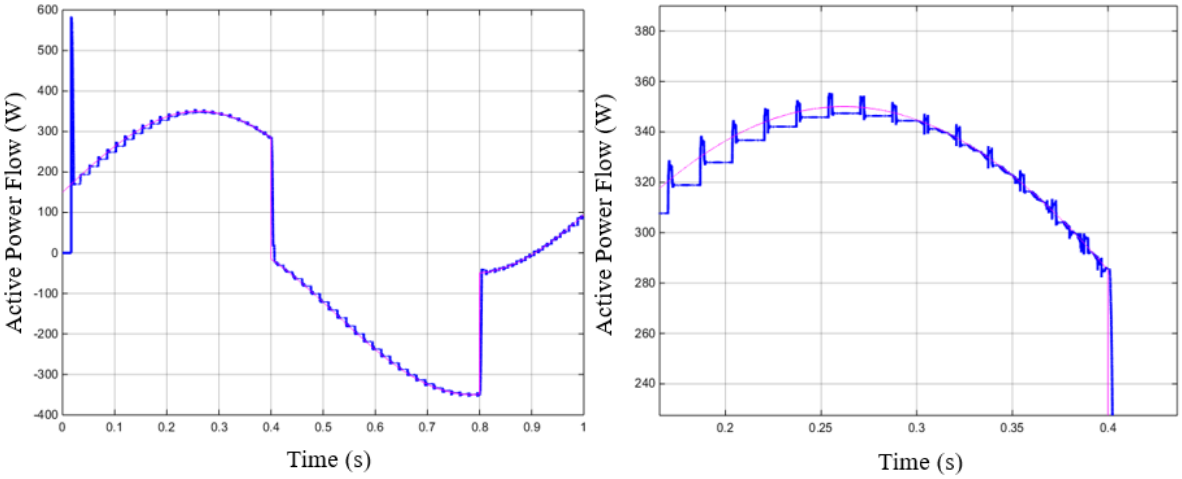

Fig. 4.20 MFAC Control System Response under Dynamic Reference Signal

In this test, ITAE is 4.746, and rise time is 0.0348. The figures indicate that MFAC system has good tracking ability and quick response ability for changing reference signal. However, the stable stage performance is not very satisfying, overshot could be large as 0.03% at some points. Compared with the control performance of constant reference and PID controller, MFAC control system could mostly meet the requirement for the power flow control system set in chapter 1. But in real world, disturbances exist everywhere, to generalize the implementation of MFAC control system, performance under practical disturbance need to be tested, so further simulations are performed on the stability and robustness.

4.4.4 Disturbance Simulation

There are countless sources and kinds of noise and disturbances in real-world industrial applications. They could be categorized into measurement disturbance and load disturbance according to their influence on different parts of the production process or be categorized into high-frequency noise and low-frequency noise according to their frequency.

1) Measurement Disturbance

a) Internal Noise Source

Component noise: Component noise is caused by the electronic random thermal movement within conductor device or semiconductor device within the control system, which is called thermal noise or Johnson noise. The power spectrum is proportional to the absolute temperature of semiconductor components, and it is typical white noise.

Mechanical noise: Mechanism noise is caused when the mechanism of the instrument measurement system is imperfect, or the assumptions cannot be fully satisfied. The measured value will be different from the theoretical value.

b) External Noise Source

There are a lot of high-voltage transmission line equipment in industrial control sites. The ionization and discharge of air near these high-voltage circuits will bring a lot of random noise to measuring instruments or sensors. The main method to suppress measurement noise in the control system is filtering, to filter the sampled signal.

2) Load disturbance

Load disturbance refers to the disturbance signal generated by the load during the operation of the system. Load disturbance can happen on both the input and output of the system, including input load disturbance and output load disturbance. Load disturbance signals could exist in many different forms, including constant signals, periodic signals (sinusoidal models, harmonic signals, etc.), and random noise signals.

There are a lot of disturbance source in the real-world AC/DC converter system. For component noise, IGBT and transformer will generate heat which will cause thermal loss

during working. And for IGBT, the conduct and disconnect, switching process is not ideal in real world, especially under high switching frequency circumstance. For transformer, there is power loss during voltage conversion; for mechanical noise: measurement of active power and shift phase ratio for control loop; for load disturbance, random noise from high voltage transmission on the I/O signal. What's more, Since the converter system is designed for high voltage power transmission, the magnetic field will cause disturbance for the system.

For all those disturbances, in order to implement them during simulation, this design divides them into load disturbance and measurement disturbance based on their different influence part in the control loop as shown in Fig. 4.21, in where *d(k)* stands for load disturbance and *w(k)* stands for measurement disturbance.

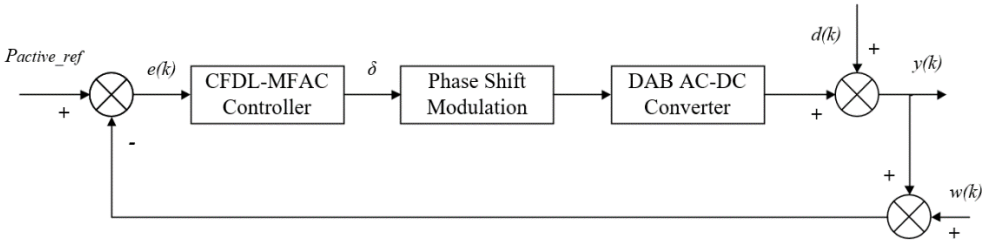

Fig. 4.21 Disturbances in MFAC Power Control System

The disturbances are generally white noise, colored noise or their combination based on diverse power spectrum. In this design, measurement disturbance is generalized as Gauss white noise and load noise is generalized as Gauss colored noise. High frequency Gauss white noise source is simulated by Band-Limited White Noise Block in Simulink with Power Spectral Density of 10 and its waveform is shown in Fig. 4.22.

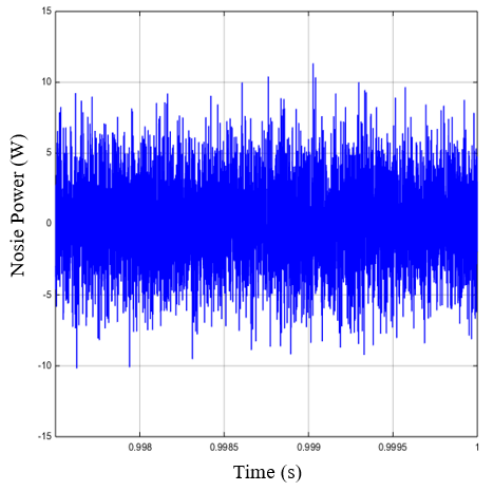

Fig. 4.22 High Frequency Gauss White Noise

High frequency Gauss colored noise could be simulated by put white noise through colored filter. In this design, it's simulated by a white noise source go through two colored filters which have the transfer function as equation 4.7 and waveform shown in Fig. 4.23.

$$G(s)=\frac{s+1}{100s+1} \tag{4.7}$$

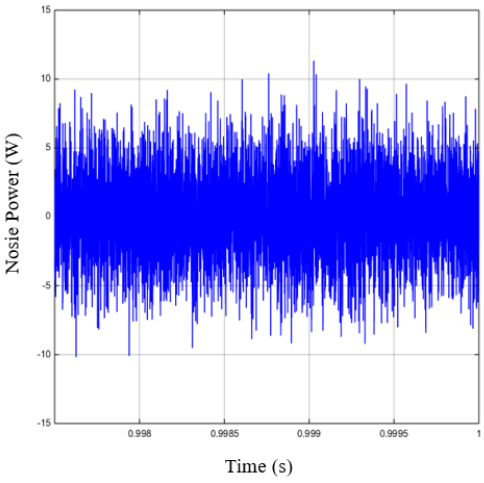

Fig. 4.23 High Frequency Gauss Colored Noise

4.4.5 Stability and Robustness Test

Stability of a control system is defined as the ability of one system to provide a bounded output when a bounded input is applied to it. A control system with strong stability is expected to be convergence under multiply disturbance on input side. To test the stability of the MFAC control system, disturbances designed in session 4.4.4 are applied to the input of this system. Meanwhile, to further explore the impact of different kinds of noise, three simulations with load disturbance, measurement disturbance, combination of load and measurement disturbance are performed based on the same conditions and model in functionality test, respectively. The results are shown in Fig. 4.24 to Fig. 4.26.

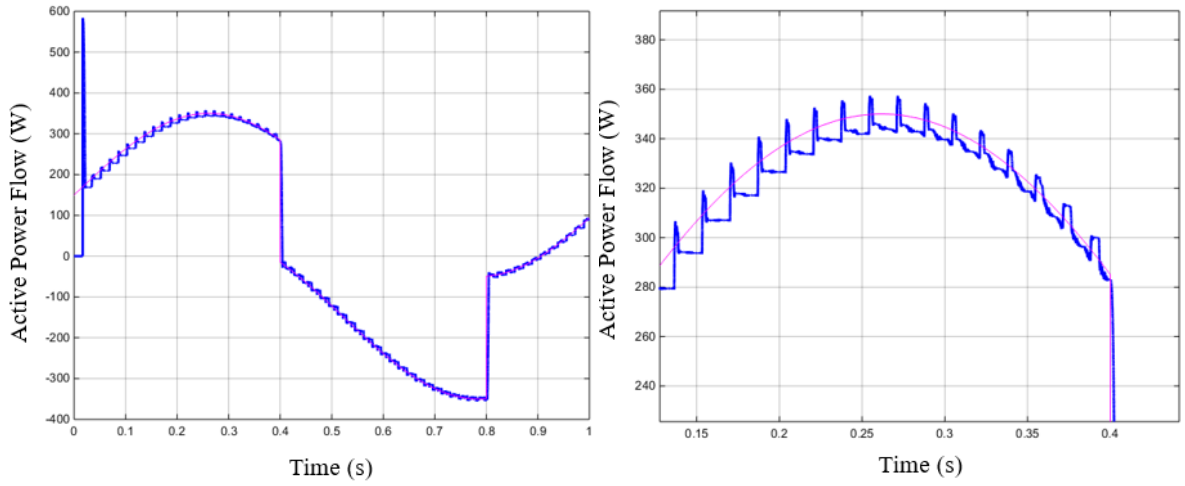

Fig. 4.24 MFAC Control System Response with Measurement Disturbance

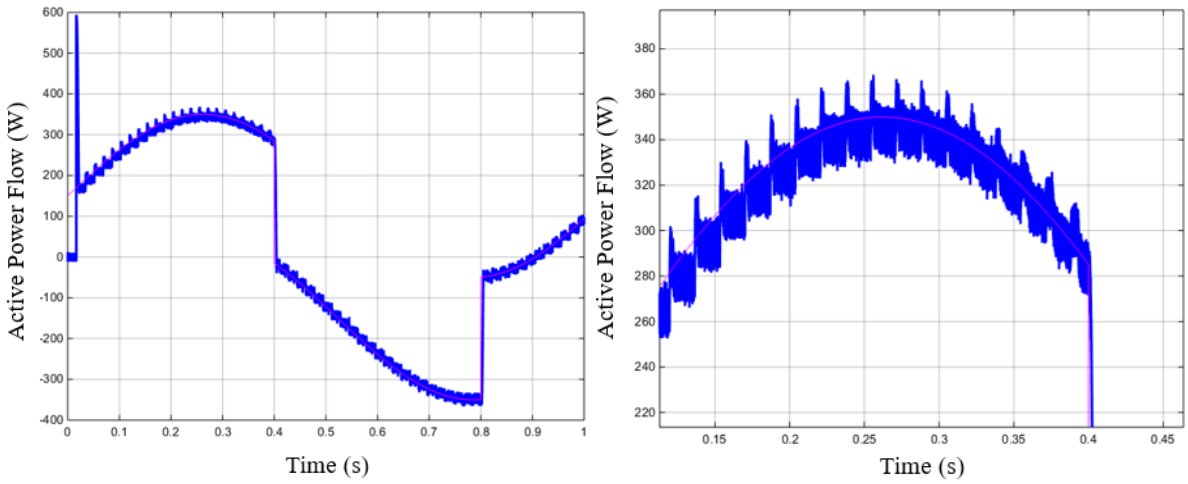

Fig. 4.25 MFAC Control System Response with Load Disturbance

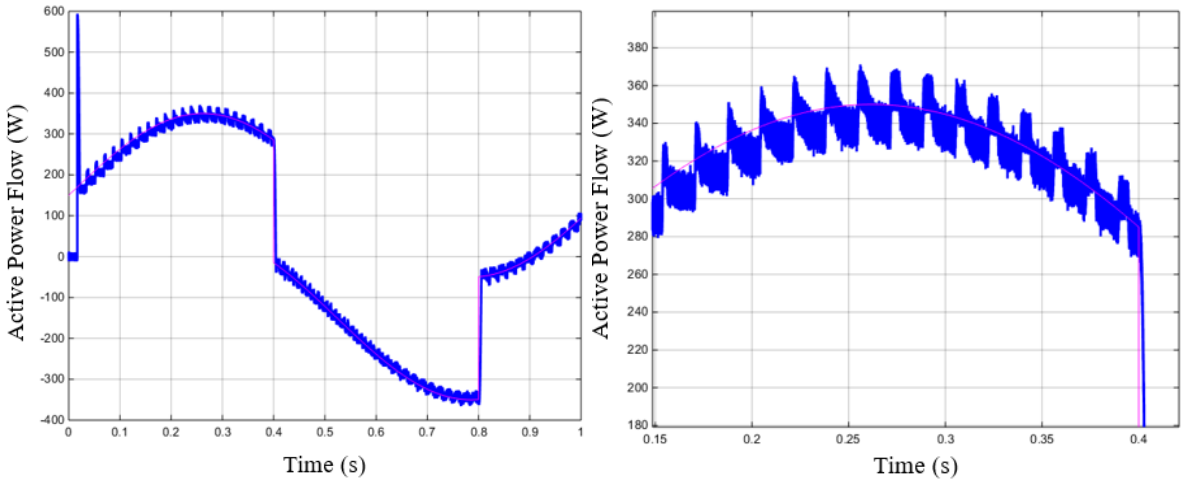

Fig. 4.26 MFAC Control System Response with Load and Measurement Disturbance

The index values of the three simulations above are: 1) ITAE is 12.83, rise time is 0.1038, 2) ITAE is 12.83, rise time is 0.1703 and 3) ITAE is 1.855 and rise time is invalid since in most of the iterations, the error is bigger than the restriction of the rise time. The results indicate that under different types of disturbance, MFAC control system could remain converging and have bounded output. However, impacts on the performance exist which leads to bigger ITAE value and longer rise time. Therefore, to eliminate those influences caused by disturbance, certain methods like filtering are supposed to be applied on this system. The

filtered-MFAC control system will be designed and tested to achieve better robustness and control performance.

4.4.6 Disturbance Rejection Test

According to the filtered-MFAC control system structure derived in session 3.3.4. A low pass filter is supposed to be applied on the error signal *e*, to filter the disturbances. A Low pass filter with cut-off frequency of 20kHz is designed by using butterworth method is employed, and the results are shown in Fig. 4.27 to Fig. 4.29.

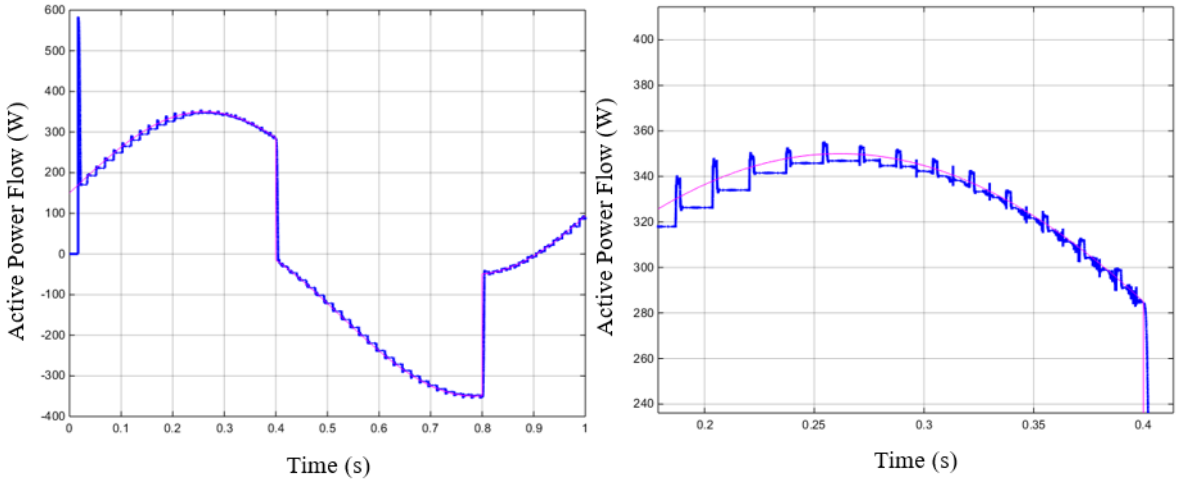

Fig. 4.27 Filtered-MFAC Control System Response with Measurement Disturbance

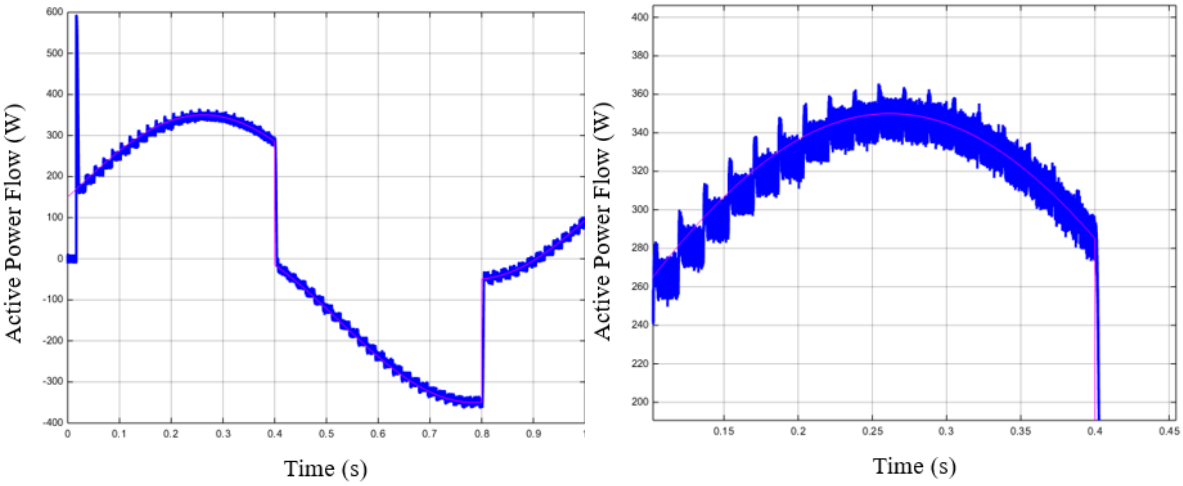

Fig. 4.28 Filtered-MFAC Control System Response with Load Disturbance

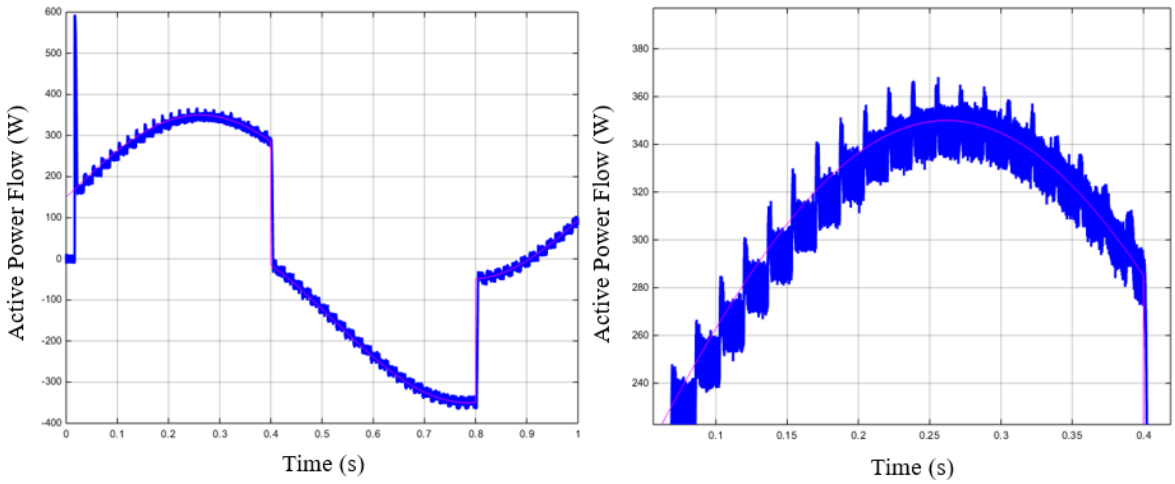

Fig. 4.29 Filtered-MFAC Control System Response with Load and Measurement Disturbance

The index values of the three simulations above are: 1) ITAE is 10.36, rise time is 0.0347, 2) ITAE is 10.64, rise time is 0.2116 and 3) ITAE is 11.64 and rise time is 0.0379. From the first two simulations, results show that filtered-MFAC has better performance than traditional MFAC, however, the improvement is not very significant. But in the third simulation, when load and measurement disturbance exist at the same time, ITAE value dropped from 18.55 to 11.64 and rise time is stable about 0.0379 which proves filtered-MFAC has better control performance under multiply disturbance. To achieve better performance, filter design needs to be further discussed.

Chapter 5: Conclusion and Recommendation for Future Work

5.1 Conclusion

This thesis presents a design process and simulation validation of a Model-Free Adaptive power flow control system based on Single-Stage Dual-Active-Bridge-Based AC/DC converter system with single H-bridge phase shift modulation. The proposed MFAC control system is able to control the direction and magnitude of the active power flow. This process is achieved by modulating the phase shift ratio between the primary and secondary side voltage of the converter without using any model information. The simulation result shows that MFAC control system could respond to the dynamic changes on both the power grid side and EES systems side quickly and accurately and has better performance, including shorter response time, stronger target signal tracking ability and disturbance rejection capability compared to PID control system. Weighting parameters and initials conditions of MFAC control system are optimized to maximize the controller functionality. Finally, a disturbance suppression MFAC control system with filtering is utilized to improve the robustness and stability, and achieve higher conversion efficiency.

5.2 Recommendation for Future Work

In general, the proposed power flow control system could control the bidirectional power flow effectively and has better performance than the traditional PID control system. However, several improvements that may further increase the robustness and efficiency of the MFAC control system are listed as following:

1) Multiple Parameters Control System Design: the controlled system is a SISO system with one input. However, this could be achieved only when duty cycle d_{dc} is

fixed since SHBM has two degrees of freedom. In real-world, many modulation strategies utilize more than two degrees of freedom to achieve higher efficiency and better performance. In this case, high-dimension algorithms that are able to simultaneously optimize several variables could be employed to control MISO or MIMO system.

2) Efficient Disturbance Rejection Methods: In this design, filtered CDFL-MFAC is employed to reject multiple disturbances and has been proved functional by simulations. However, as a data-driven algorithm, it is difficult for MFAC to further reduce the white noise disturbance. Thus, better disturbance rejection methods, like building disturbance observer and adding disturbance compensation, could be applied to achieve higher efficiency and reduce the power loss during conversion process.

Reference

[1] X. Zhang, “Study on optimazition of energy structure and countermeasures of new energy development during “ The twelfeth five-year plan” Master. dissertation, Shandong University of Science and Technology, Shandong, 2011.

[2] J. Everts, F. Krismer,V. D. K. Jeroen, J. Driesen, and J. W. Kolar, “Optimal ZVS Modulation of Single-Phase Single-Stage Bidirectional DAB AC–DC Converters,” *IEEE Trans. Power Electron.*, vol. 29, no. 8, pp. 3954-3970, Aug. 2014.

[3] M. Nebert, H. Hoek, J. Gottschlich, and R. W. D. Doncker, “Soft-switching operation strategy for three-phase multiport-active bridge DC-DC converters,” *2017 IEEE 12th International Conference on Power Electronics and Drive Systems (PEDS)*, 2017, pp. 2164-5264.

[4] S. Norrga, “Experimental Study of a Soft-Switched Isolated Bidirectional AC–DC Converter Without Auxiliary Circuit,” *IEEE Trans. Power Electron.*, vol. 21, no.6, pp. 1580-1587, 2006.

[5] B. Zhao, Q. Song, W. Liu, and Y. Sun, “Overview of Dual-Active-Bridge Isolated Bidirectional DC-DC Converter for High-Frequency-Link Power-Conversion System,” *IEEE Trans. Power Electron.*, vol. 29, no. 8, pp. 4091-4107, Aug. 2014.

[6] R. De Doncker, D. Divan, and M. Kheraluwala, “A three-phase soft- switched high-power-density dc/dc converter for high-power applica- tions,” *IEEE Trans. Ind. Appl.*, vol. 27, no. 1, pp. 63–73, Jan./Feb. 1991.

[7] M. Kheraluwala, R. Gascoigne, D. Divan, and E. Baumann, “Performance characterization of a high-power dual active bridge dc-to-dc converter,” *IEEE Trans. Ind. Appl.*, vol. 28, no. 6, pp. 1294–1301, Nov./Dec. 1992.

[8] B. Zhao, Q. Song, and W. Liu, “Power characterization of isolated bidirec- tional dual-active-bridge dc-dc converter with dual-phase-shift control,” *IEEE Trans. Power Electron.*, vol. 27, no. 9, pp. 4172–4176, Sep. 2012.

[9] Y. Wang, S. W. H. De Haan, and J. Ferreira, “Optimal operating ranges of three modulation methods in dual active bridge converters,” in *Proc. IEEE Power Electron. Motion Contr. Conf. (IPEMC ’09)*, 2009, pp. 1397–1401.

[10] G. Oggier, G. Garcia, and A. Oliva, “Switching control strategy to minimize dual active bridge converter losses,” *IEEE Trans. Power Electron.*, vol. 24, no. 7, pp. 1826–1838, Jul. 2009.

[11] G. Oggier, G. Garcia, and A. Oliva, “Modulation strategy to operate the dual active bridge dc-dc converter under soft switching in the whole operating range,” *IEEE Trans. Power Electron.*, vol. 26, no. 4, pp. 1228– 1236, 2011.

[12] Z. Hou and S. Jin, “Model free adaptive control theory and application,” Academic: CRC Press, 2014.

[13] Z. Hou and S. Xiong, “On model-free adaptive control and its stability analysis,” *IEEE Transactions on Automatic Control*, vol. 64, no. 11, pp. 4555-4569, Jan. 2019.

[14] E. Panteley and A. Loria, “On global uniform asymptotic stability of nonlinear time-varying non-autonomous systems in cascade,” *Systems and Control Letters (S0005-1098)*, vol. 33, no. 2, pp. 131-138, 1998.

[15] P. Ma, W. Li, G. Zheng, and Y. Niu, “The application of model free adaptive control,” *IMACS Multiconference on "Computational Engineering in Systems Applications"*, 2006, pp. 393-396.

[16] F. Krismer and J. Kolar, “Closed form solution for minimum conduction loss modulation of dab converters,” *IEEE Trans. Power Electron.,* vol. 27, no. 1, pp. 174–188, Jan. 2012.

[17] K. Vangen, T. Melaa, and A. Adnanes, “Soft-switched high-frequency, high power dc/ac converter with IGBT,” in *Proc. IEEE Power Electron. Spec. Conf.,* Jun. 29–Jul. 3, 1992, vol. 1, pp. 26–33.

[18] F. Krismer, S. Round, and J. Kolar, “Performance optimization of a high current dual active bridge with a wide operating voltage range,” in *Proc. IEEE Power Electron. Spec. Conf.*, 2006, pp. 1–7.

[19] Y. Wang, S. W. H. De Haan, and J. Ferreira, “Optimal operating ranges of three modulation methods in dual active bridge converters,” in *Proc. IEEE Power Electron. Motion Contr. Conf. (IPEMC ’09),* 2009, pp. 1397–1401.

[20] F. Jauch and J. Biela, “Combined phase-shift and frequency modulation of a dual-active-bridge ac–dc converter with PFC,” *IEEE Trans. Power Electron.,* vol. 31, no. 12, pp. 8387-8397, Dec. 2016.

[21] H. Tao, A. Kotsopoulos, J. Duarte, and M. A. M. Hendrix, “Transformer-coupled multiport ZVS bidirectional dc-dc converter with wide input range,” *IEEE Trans. Power Electron.*, vol. 23, no. 2, pp. 771–781, Mar. 2008.

[22] J. H. Youm and B. H. Kwon, “Switching technique for current-controlled AC-to-AC converters,” *IEEE T. Ind. Electron,* vol. 46, pp. 309–318, 1999.

[23] N. D. Weise, G. Castelino, K. Basu, and N. Mohan, “A single-stage dual-active-bridge-based soft switched ac–dc converter with open-loop power factor correction and other advanced features,” *IEEE Trans. Power Electron.*, vol. 29, no. 8, pp. 4007-4016, Aug. 2014.

[24] G. Castelino, K. Basu, N. D. Weise, and N. Mohan, “A bi-directional, isolated, single-stage, DAB-based AC-DC converter with open-loop power factor correction and other advanced features,” in *IEEE International Conference on Industrial Technology*, 2012, pp. 938-943.

[25] Z. Hou and Z. Han, “Robust modelless learning adaptive control of nonlinear systems,” *Control and Decision*, vol. 10, no. 2, pp. 137-142, Mar. 1995.

[26] Z. Hou and S. Xiong, “On model-free adaptive control and its stability analysis,” *IEEE Transactions on Automatic Control*, vol. 64, no. 11, pp. 4555-4569, Nov, 2019.

[27] Z. Hou and J. Xu, “On data-driven control theory: the state of the art and perspective,” *Acta Automatica Sinica*, vol. 35, no. 6, pp. 650-667, 2009.

[28] X. Bu, Z. Hou, and S. Jin, “The robustness of model-free adaptive control with disturbance suppression,” *Control Theory & Applications*, vol. 28, no. 3, pp. 358-362, Mar. 2011.

[29] F. Xu, D. Li, and Y. Xue, “Comparing and optimum seeking of PID tuning methods base on IATE index,” *Proceediings of CSEE*, vol. 23, no. 8, pp. 206-210, Aug. 2003.

Appendix A

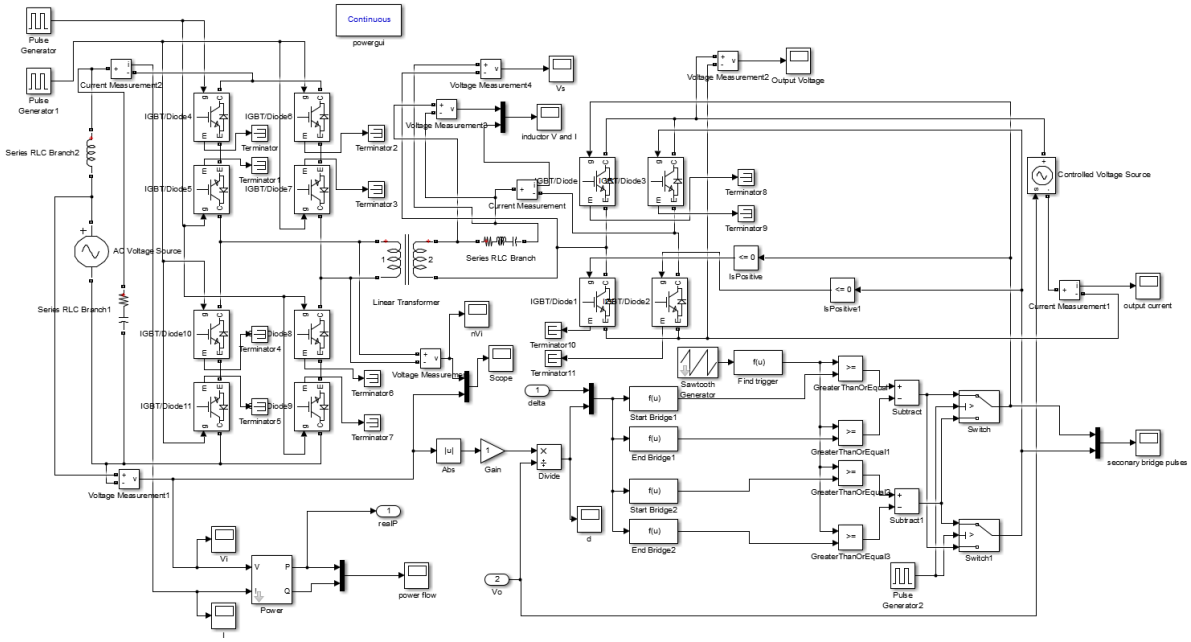

Figure 1. DAB AC/DC Converter Simulink Model

Appendix B

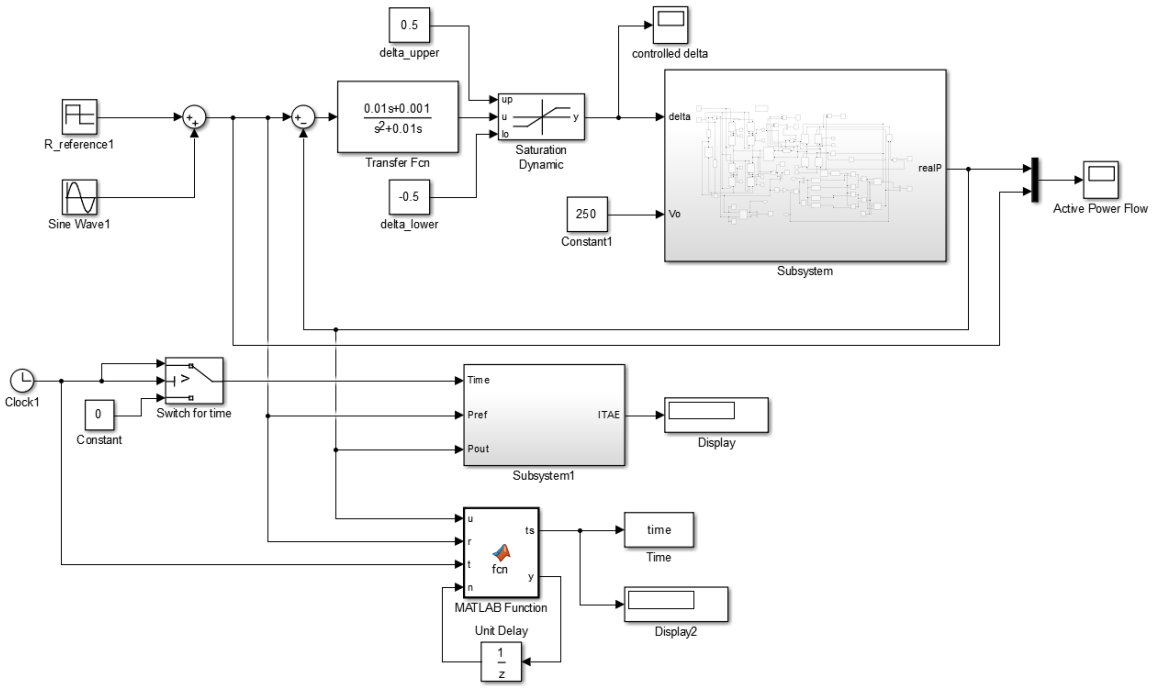

Figure 2. PID Power Flow Control System Simulink Model

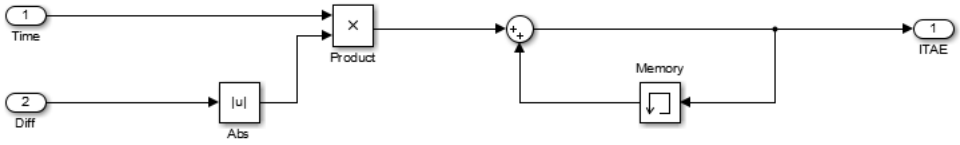

Figure 3. ITAE Calculation Code

Appendix C

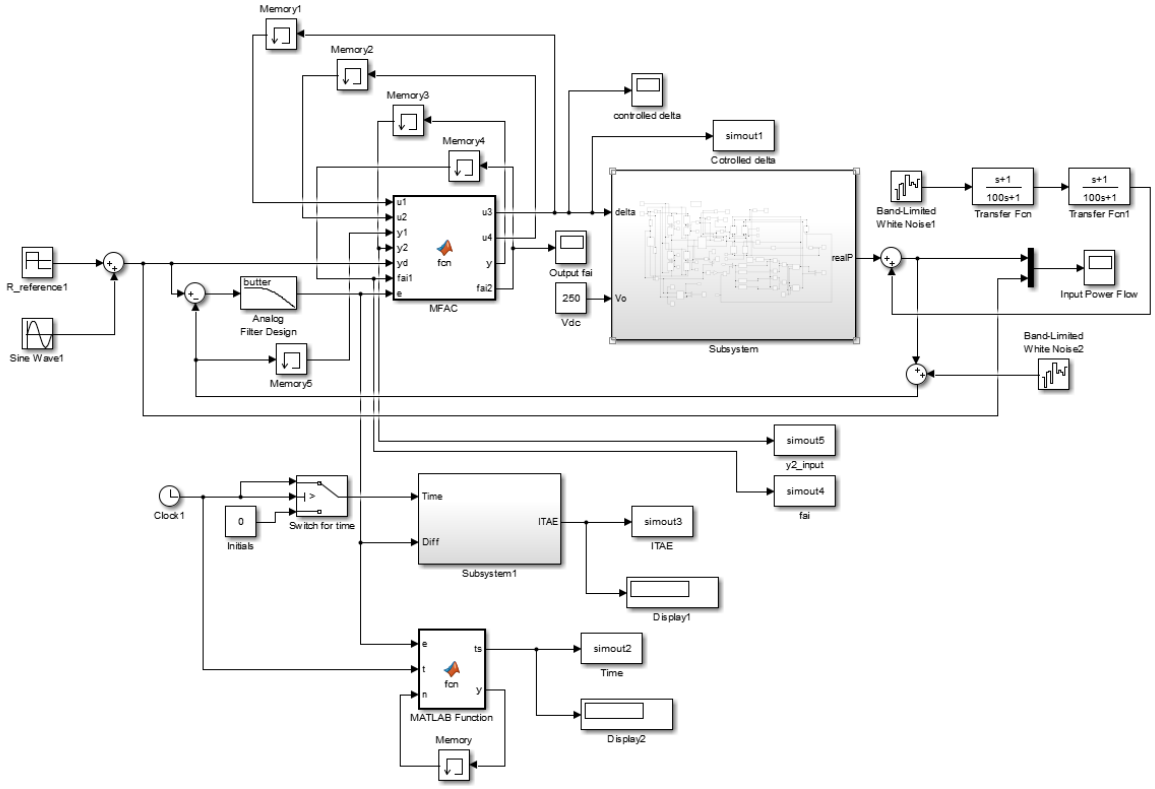

Figure 4. MFAC Power Flow Control System Simulink Model

Appendix D

The code for MFAC implementation:

```
function [u3,u4,y,fai2] = fcn(u1,u2,y1,y2,yd,fai1,e)
% Assum this is the kth iteration
% Input variables                          OutPut variables
% u1        u(k-1)                           u3          u(k)
% u2        u(k-2)                           u4          u(k-1)
% y1        y(k)                             y           y(k)
% y2        y(k-1)                           fai2        fai(k)
% yd        yd(k+1) reference signal
% fai1      fai(k-1)
% e         filtered difference

% Control parameters
eita =1; miu =1; rou=1; lamda =1;

% Find PPD based on the inputs
fai2 = fai1 + eita*((y1-y2)-fai1*(u1-u2))*(u1-u2)/(miu+(u1-u2)*(u1-u2));
if (fai2 <10^(-5)) || (((u1-u2)*(u1-u2))^0.5<10^(-5))
      fai2=0.1;
end
% Derivative the next output
u3 = u1 + rou*fai2*(e)/(lamda+fai2^2);

if u3 < -0.5
      u3 = -0.5;
else if u3 > 0.5
            u3 = 0.5;
      else
            u3 = u3;
      end
end

u4 = u1; y = y1;
end
```

The code for Benchmark function test:

```
clear all;
%close all;
N=500;
```

```
%Control parameters
nu=1;
eita =0.5; %(0,2]
miu =1; % >0
rou=0.5; %(0,1]
lamda =0.1; %>0

%initial conditions
y(1)=1;y(2)=0.5;y(3)=-1;
u(1:2)=0;
du(1:2,1:nu)=0;
%reference
for k=1:N+1
    yd(k)=Griewank(k);
end
I=eye(nu);
% fai(1:nu,1) =2;
% fai(1:nu,2:nu)=0;
fai(1:2,1) =[1 3];
fai(1:2,2:nu)=0;
%for k=nu+1:N
for k=3:N
    a(k)=1+round(k/500);
    fai(k,1:nu)=fai(k-1,1:nu)+eita*(y(k)-y(k-1)-fai(k-1,1:nu)*du(k-1,1:nu)')*du(k-
1,1:nu)/(miu+du(k-1,1:nu)*du(k-1,1:nu)');
    if (fai(k,1)<10^(-5)) || ((du(k-1,1:nu)*du(k-1,1:nu)')^0.5<10^(-5))
        fai(k,1)=0.5;
    end
    if nu==1
        u(k) = u(k-1)+rou*fai(k,1)*(yd(k+1)-y(k))/(lamda+fai(k,1).^2);
    else
        u(k)=u(k-1)+rou*fai(k,1)*(yd(k+1)-y(k)-fai(k,2:nu)*du(k-1,1:nu-
1)')/(lamda+fai(k,1).^2);
    end
    %model
    if k<=500
        y(k+1)=y(k)/(1+y(k).^2)+u(k)^3;
    else
        y(k+1)=(y(k)*y(k-1)*y(k-2)*u(k-1)*(y(k-2)-1)+a(k)*u(k))/(1+y(k-1)^2+y(k-
2)^2);
    end
    for i=1:nu
        du(k,i)=u(k-i+1)-u(k-i);
```

```
        end
        emax(k+1)=yd(k+1)-y(k+1);
end

plot(1:501,yd,'r');
hold on;
grid on;
plot(1:501,y,'b');
legend('Expected Signal','Tracking Signal');
xlabel('Iteration');
ylabel('Value');

function [itae] = Griewank(x)
%Griewank:[-600,600],f(0)=0
A=0;
B=1;
A=A+x^2;
B=B*cos(x);
itae=1/4000*A-B+1;
end
```